Journal of Neuroscience Methods, 49 (1993) 157–165

NSM 01535

Injection of digitally synthesized synaptic conductance transients to measure the integrative properties of neurons

Hugh P.C. Robinson [a] and Nobufumi Kawai [b]

[a] *Physiological Laboratory, University of Cambridge, Downing St., Cambridge, CB2 3EG (UK) and* [b] *Department of Physiology, Jichi Medical School, Minamikawachi, Tochigi-ken 329-04 (Japan)*

(Received 5 January 1993)
(Revised version received 8 April 1993)
(Accepted 14 April 1993)

Key words: Conductance injection; Synaptic conductance; Current-clamp; Hippocampal neuron

A novel technique was developed for injecting a time-varying conductance into a neuron, to allow quantitative measurement of the processing of synaptic inputs. In current-clamp recording mode, the membrane potential was sampled continuously and used to calculate and update the level of injected current within 60 μs, using a real-time computer, so as to mimic the electrical effect of a given conductance transient. Cellular responses to synthetic conductance transients modelled on the fast (non-*N*-methyl-D-aspartate) phase of the glutamatergic postsynaptic potential were measured in cultured rat hippocampal neurons.

Introduction

The inputs to a neuron consist of focal transients of membrane conductance at the postsynaptic sites, whose magnitude is essentially independent of the postsynaptic response. The output of a neuron is represented by the membrane potential in the cell body or axon. However, the relationship between transient conductance inputs and the resulting trajectory of membrane potential has never been directly measured. The current $I_{syn}(t)$ flowing through the synaptic conductance at a postsynaptic site depends on the postsynaptic membrane potential $V(t)$, according to the equation

$$I_{syn}(t) = g(t)(E_{rev} - V(t)) \quad (1)$$

where $g(t)$ is the time-varying conductance and E_{rev} is the reversal potential for the conductance. In particular, for a given $g(t)$, the current is diminished to zero and then reversed as the membrane is polarized through E_{rev}. $V(t)$ depends upon the complexities of current flow throughout the whole neuron, including $I_{syn}(t)$, active voltage-dependent currents, and currents at other synaptic sites. The interdependence of $I_{syn}(t)$ and $V(t)$ is such that, even for a passive membrane consisting of a linear resistance and capacitance in parallel, the conductance input-voltage output relationship is non-linear. Furthermore, injection of a fixed-current transient, without feedback of the membrane potential cannot, in general, reproduce the effect of a conductance input. Nevertheless, current injection has been the main technique employed to gain experimental insight into the integrative action of mammalian neurons (for a review, see Llinás, 1988). The assumption that synaptic inputs are prescribed current transients also greatly simplifies the problem of calculating voltage responses for

Correspondence: Hugh P.C. Robinson, Physiological Laboratory, University of Cambridge, Downing St., Cambridge, CB2 3EG, UK. Tel.: 0223-333835.

passive membrane, which becomes linear (Rall, 1977). However, as seen from Eqn. 1, this approach can be valid only when the voltage is so far from the equilibrium potential that it can be considered constant. It cannot describe even approximately the action of an inhibitory synapse as the membrane potential ranges on both sides of the reversal potential. The analytical theory of conductance inputs for passive membrane is extremely difficult, and has not so far provided general solutions analogous to those for current inputs (MacGregor, 1968; Barrett and Crill, 1974; Poggio and Torre, 1978; Tuckwell, 1988). Numerical modelling has been the most profitable approach to defining the role of conductance inputs (e.g., Koch et al., 1983; Turner, 1984; Wathey et al., 1992), but relies upon still fragmentary knowledge of the properties and distributions of neuronal membrane conductances.

In order to characterize the integrative action of neurons experimentally, it is necessary to measure the output $V(t)$ in response to exactly specified transients of conductance at defined locations in the cell, which have the same kinetics and reversal potential as natural synaptic conductance transients. Neither voltage-clamp nor current-clamp techniques provide a direct approach to this problem. Voltage-clamp recording, in measuring $g(t)$, necessarily cancels $V(t)$, while current-clamp recording measures $V(t)$ but not $g(t)$. Here, we present a technique for stimulating a neuron, during current-clamp recording, with a current that follows Eqn. 1. This has the effect of simulating a known transient *conductance*, and allows the $g(t)/V(t)$ relationship to be measured explicitly. In this technique, the injected current level is continuously updated according to Eqn. 1 by a real-time computer, using the instantaneous measurement of the membrane potential, a prespecified constant reversal potential and a time template for the conductance derived from voltage-clamp recordings of synaptic currents. The method was applied in small cultured hippocampal neurons to demonstrate the processing of conductance transients mimicking the natural fast excitatory and inhibitory postsynaptic conductances. A preliminary report of this work has appeared elsewhere (Robinson, 1991).

Methods

Dissociated hippocampal neurons were cultured from neonatal rats as described previously (Robinson et al., 1991), and maintained for 1–2 weeks before experiments. Very small (diameter < 12 μm), rounded neurons with few processes were selected for recording. To record natural spontaneous postsynaptic currents, pipettes were filled with the solution: 141 mM CsCl, 5 mM EGTA, 0.5 mM $CaCl_2$, 10 mM HEPES/Na (pH 7.2). The bath solution contained: 150 mM NaCl, 2.8 mM KCl, 0.5 mM $CaCl_2$, 10 mM HEPES/Na (pH 7.2). For conductance injection, the pipette solution consisted of: 141 mM KCl, 0.5 mM $CaCl_2$, 5 mM EGTA, 10 mM HEPES/Na (pH 7.2), and the bath solution of 142 mM NaCl, 2.8 mM KCl, 2 mM $CaCl_2$, 1 mM $MgCl_2$, 10 mM HEPES/Na, 5 mM D-glucose (pH 7.2) to which were added 10 μM CNQX (Tocris Neuramin, Buckhurst Hill, UK), 30 μM APV (Tocris), and 30 μM strychnine (Tokyo Kasei Kogyo Co., Tokyo, Japan). All experiments were at room temperature (23–25°C).

Conductance injection was carried out as follows. Whole-cell recordings (Hamill et al., 1981) were established using a whole-cell patch-clamp amplifier (Axopatch 1-D, Axon Instruments, Foster City, CA) in current-clamp mode. In voltage-clamp mode, the capacitive charging time constant was less than 40 μs. The real-time calculation of the current command signal was performed by a dedicated analog processing board (AS-1, Cambridge Research Systems, Rochester, Kent, UK), which included a 12 MHz 80186 processor, clocks, 512 kbytes memory, and 12-bit analog-to-digital converters (ADC) and digital-to-analog converters (DAC). The settling time constant of the DACs was approximately 1 μs. DAC update and ADC sampling were exactly synchronized using the direct memory access channels of the processor. The membrane potential signal was sampled after passage through an anti-aliasing filter (5 kHz, -3dB Bessel characteristic). Conductance templates were stored in memory at a resolution of 16 bits, and the multiplication, at each time step, by the result of subtracting the voltage from the reversal poten-

tial, was carried out to 28-bit intermediate precision. The 12 most significant bits were written to the DAC connected to the current command input of the amplifier. The arithmetic in each cycle lasted only 4.58 μs, with the remaining time used for handling timers, transferring samples to memory, and update of loop variables. The smallest attainable δt was 58.8 μs, which was used throughout.

Results

Whole-cell voltage-clamp recording from small neurons cultured from rat hippocampus revealed 2 types of spontaneous synaptic current. A glutamatergic excitatory postsynaptic current (e.p.s.c) (Fig. 1a), comprised a fast, non-*N*-methyl-D-aspartate (non-NMDA) receptor-mediated component with a decay time constant (τ) of 1.5–4 ms (Fig. 1a), and a slow, NMDA receptor-mediated phase with a decay τ of 80–150 ms (Eqn. 3) (Fig. 1b), in which single channel openings could clearly be resolved in the whole-cell current (see Robinson et al., 1991). Similar biphasic glutamatergic e.p.s.c.s have been described by Hestrin et al. (1988), Forsythe and Westbrook (1988), Bekkers and Stevens (1989) and Keller et al. (1991), and appear to be a general feature of most mammalian central neurons. An inhibitory postsynaptic current (i.p.s.c.) decayed monoexponentially with a τ of 30–40 ms (Fig. 1c), as described by Segal and Barker (1984).

We found that both the fast phase of the

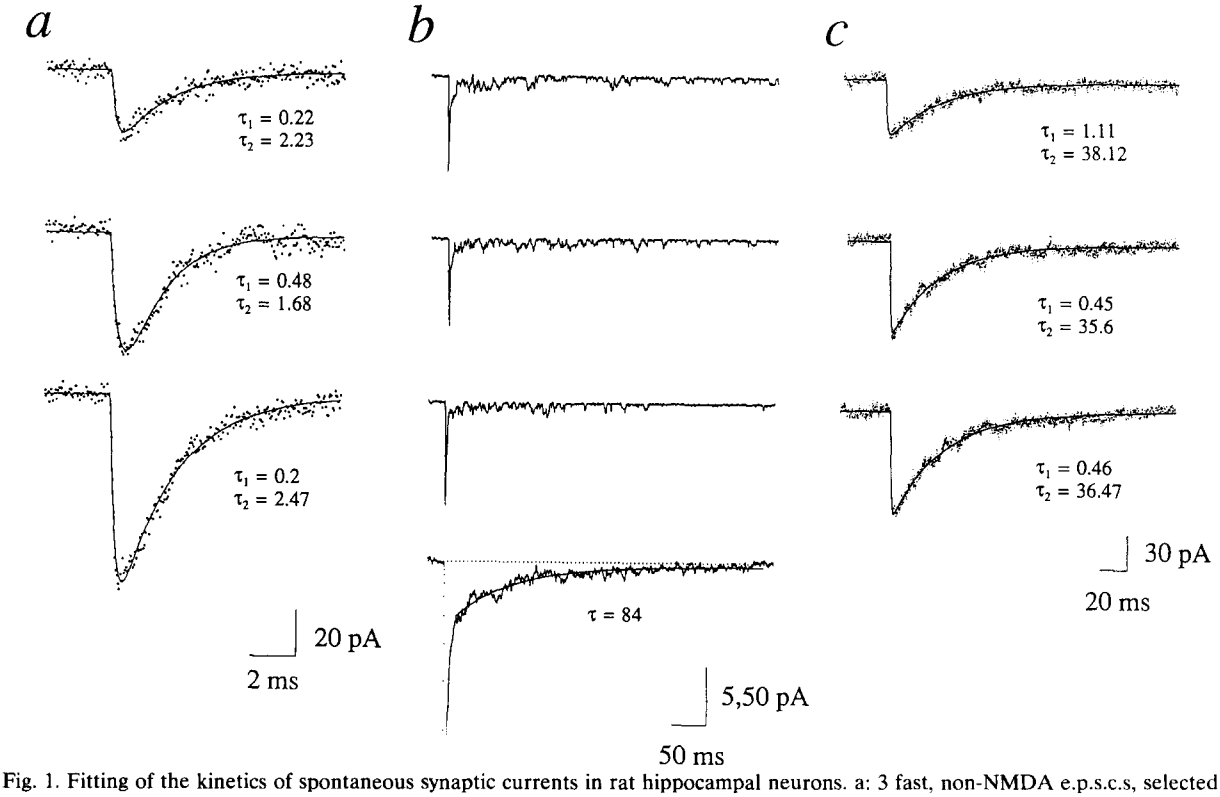

Fig. 1. Fitting of the kinetics of spontaneous synaptic currents in rat hippocampal neurons. a: 3 fast, non-NMDA e.p.s.c.s, selected for the absence of early ensuing NMDA channel openings. Least-squares fits to the equation: $I(t) = K\ (1 - \exp(-t/\tau_1))\ \exp(-t/\tau_2)\ (E_{rev} - V)$ are superimposed with the values of τ_1 and τ_2 indicated. $V = -75$ mV, bandwidth DC -10 kHz (approximate bandwidth of amplifier and recording system, resampled at 25 kHz). b (3 top traces): spontaneous e.p.s.c.s, with the characteristic biphasic appearance of the non-NMDA (fast)/NMDA (slow, noisy) glutamatergic e.p.s.c. Single channel openings may be seen in the NMDA phase. (lower trace): ensemble average of 30 aligned spontaneous e.p.s.c.s, with a single exponential fit of $\tau = 84$ ms to the slow (NMDA) phase. $V = -75$ mV, bandwidth DC -2 kHz (Gaussian). c: 3 i.p.s.c.s, with fits as in (a). $V = -70$ mV, bandwidth DC -10 kHz, as in (a).

e.p.s.c and i.p.s.c were well fitted by a product of 2 exponential functions, so that the underlying conductance transients, $g(t)$, could be written as

$$g(t) = K \cdot \left(1 - \exp\frac{-t}{\tau_1}\right) \cdot \exp\frac{-t}{\tau_2}. \qquad (2)$$

Assuming that $g(t)$ is independent of V, the current $I(t)$ flowing at the synaptic site should be given by substituting Eqn. 2 for $g(t)$ in Eqn. 1. This assumption is reasonable for the fast glutamate e.p.s.c., which shows only a 10% change in decay τ over the range -100 mV to 0 mV (Keller et al., 1991). To inject conductance transients, we used the discrete time approximation to Eqn. 1: $I_{t+\delta t} = g_t \ (E_{rev} - V_t)$, to determine the commanded current in current-clamp recording mode. At time $t + \delta t$, the commanded current level was updated to the product of the conductance value in the template for time t and the result of subtraction of the potential measured at time t from the reversal potential E_{rev}. This feedback loop has the effect of creating a current source which well approximates the effect of the synaptic conductance $g(t)$ when δt is small. In the present experiments, δt was fixed at 58.8 μs. To confirm the accuracy of the conductance synthesis, we injected conductance transients of the form specified by Eqn. 2 with $\tau_1 = 2$ ms and $\tau_2 = 15$ ms, into a model passive cell. The resulting voltage response was very close to the expected response, calculated by integrating the differential equation for the circuit numerically (Fig. 2).

Fig. 3a shows the injection of a conductance transient modelled on that of the fast e.p.s.c, with a reversal potential of 0 mV. For all conductance injection experiments, the pipette contained a predominantly potassium chloride solution (see Materials and methods), while CNQX, APV, strychnine and magnesium were added to the bath. The intention was to block natural synaptic events without impairing the function of voltage-dependent channels which react to synaptic conductance inputs under physiological conditions; it should be noted that strychnine is an effective blocker not only of glycine receptors, but also of $GABA_A$ receptors at the concentration used (30 μM) (Shirasaki et al., 1991). The measured potential is shown superimposed on the expected

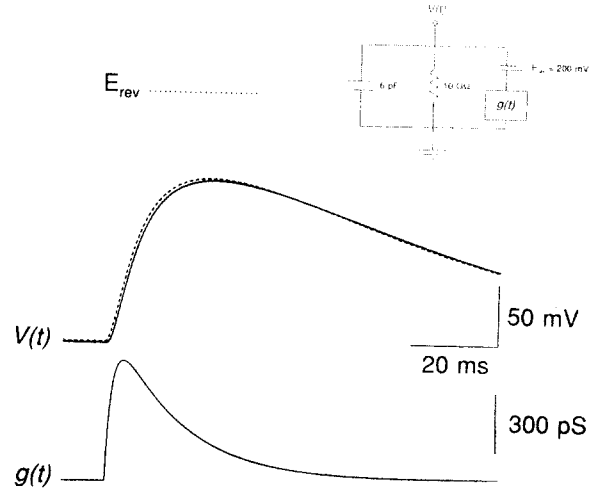

Fig. 2. Conductance injection in a model cell. $g(t)$ was specified by Eqn. 2, with $K = 900$ pS, $\tau_1 = 2$ ms, $\tau_2 = 15$ ms, $E_{rev} = 200$ mV (indicated by a dotted line). The parameters of the model cell are shown in the inset. The solid $V(t)$ trace shows the measured response (average of 10 trials), while the dashed trace shows the expected response calculated by numerical integration (Euler integration, time step 1 μs).

passive response calculated by numerical integration, using the values for cell input resistance and capacitance determined by small hyperpolarizing current steps from rest (see Fig. 3a inset). This reveals a non-linear active response due to voltage-dependent inward current. The injected current is the product of the time-varying potential driving force and the conductance template, and reaches its peak approximately 0.5 ms before the peak of conductance, then falls biphasically before rising again in a small, late peak. Thus, current of a similar time course should flow through the non-NMDA channels during a synaptic potential in the unclamped active membrane. In Fig. 3b, a conductance template based on the slower kinetics of an inhibitory postsynaptic event, and a reversal potential of -60 mV, was injected repeatedly as the membrane potential was changed between -100 and -25 mV by background current injection, illustrating the reversal of the artificially induced transients.

The relationship between the amplitude of a fast glutamate-like conductance transient and the depolarization was investigated by varying K (Fig. 4a). At potentials near to rest, the form of re-

sponses is as expected for a passive membrane, and the peak of each response showed the gradual sublinearity expected as the driving force was reduced by approaching E_{rev}. Around -35 mV, a graded action potential appeared, whose peak becomes higher and earlier with increasing K. Graded action potentials are also observed in small cultured hippocampal neurons when stimulated by conventional current injection (Johannson et al., 1992). From the plot of the peak of $V(t)$ against K (Fig. 4b), the resistance of this cell appears to be higher in the depolarizing direction than measured at rest, possibly due to the presence of inward rectifier K^+ channels. Similar peak $V(t) - K$ relationships were found in 3 other neurons. Fig. 5 shows the effect of varying the kinetics of the conductance transient, in the same neuron as in Fig. 4. When the 2 time constants in Eqn. 2 were multiplied by the same scaling factor, (scaling in time only, without change in the peak conductance), the maximum depolarization at each value of K increased markedly as the kinetics were scaled from $\tau_1 = 0.5$, $\tau_2 = 2$ ms, up to $\tau_1 = 3$, $\tau_2 = 12$ ms, but showed comparitively little further change at $\tau_1 = 4$, $\tau_2 = 16$ ms.

Temporal summation was investigated in 1 neuron by varying the separation between 2 identical excitatory conductance transients (Fig. 6). For $K = 300$ pS, separations of 10 ms and over were subthreshold for eliciting an action potential. At smaller separations, however, a late action potential was elicited, which increased in amplitude to a maximum at 5 ms separation, declining sharply again as the separation was decreased further, though the peak value of injected conductance continued to increase. Thus, there was a sharply defined optimal separation of 5 ms. The temporal summation experiments

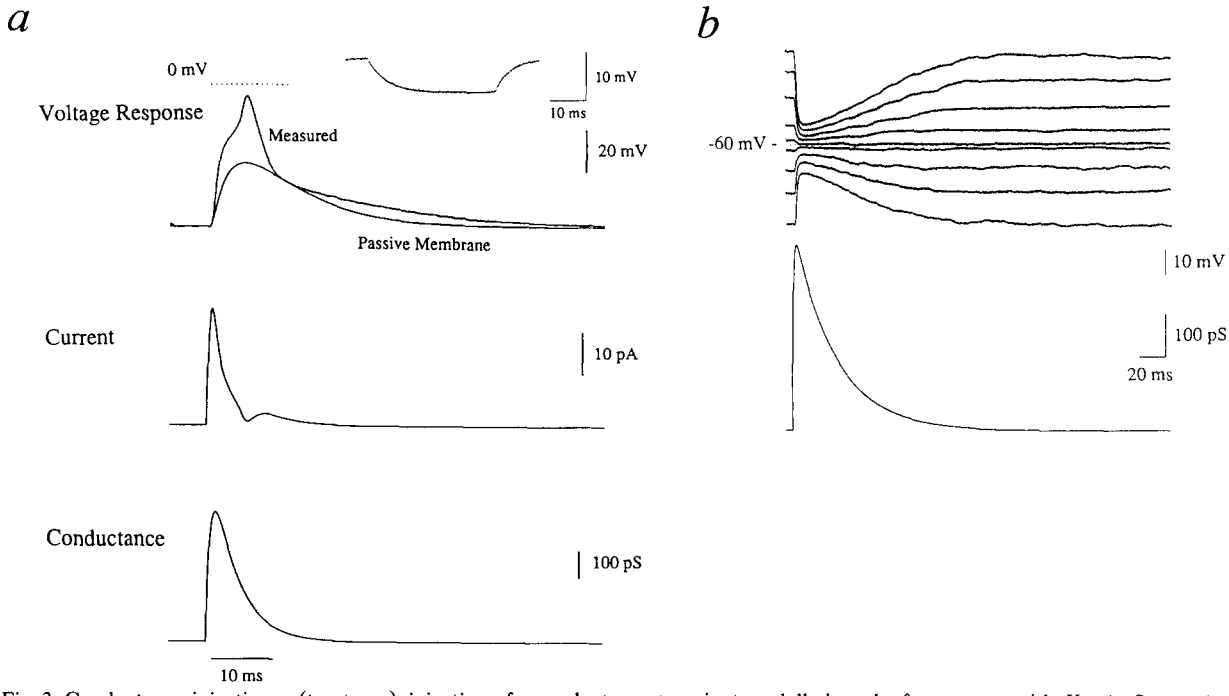

Fig. 3. Conductance injection. a (top trace): injection of a conductance transient modelled on the fast e.p.s.c., with $K = 1$ nS, $\tau_1 = 1$, $\tau_2 = 4$, $E_{rev} = 0$ mV; (top trace): measured voltage response superimposed on the expected response (calculated by numerical integration) if the cell comprised a 3.79 GΩ resistor and a 2.2 pF capacitor in parallel; values measured using 1.4 pA hyperpolarizing current steps from rest (inset). (middle trace): the (commanded) current injected during the transient, determined by the equation: $I_{t+\delta t} = g_t (E_{rev} - V_t)$. δt was 58.8 μs. b: voltage responses to injection of a g_t template modelled on the i.p.s.c. (bottom trace): $K = 500$ pS, $\tau_1 = 1$ ms, $\tau_2 = 30$ ms, $E_{rev} = -60$ mV. The resting membrane potential was varied for each different voltage response by injection of an additional constant background current. Cell resistance, 3.5 GΩ; capacitance, 1.71 pF.

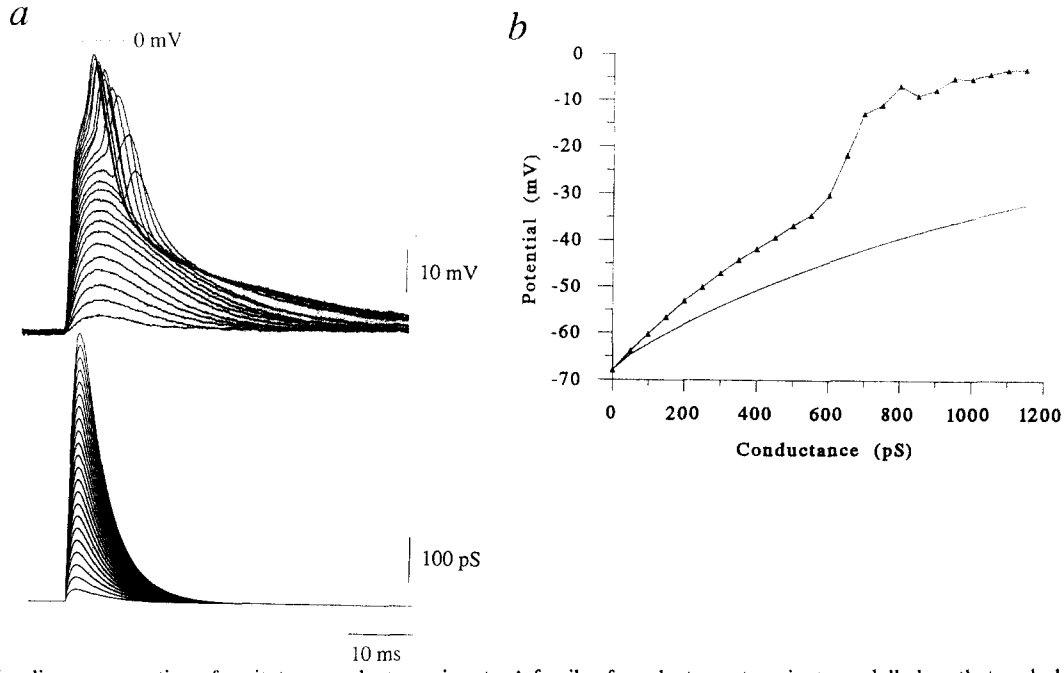

Fig. 4. Non-linear summation of excitatory conductance inputs. A family of conductance transients modelled on that underlying the fast glutamatergic e.p.s.c. ($\tau_1 = 1$ ms, $\tau_2 = 4$ ms, $E_{rev} = 0$ mV) was injected into a neuron with a resting potential of -65 mV. Each injection was separated by 10 s for recovery, and K was stepped from 50 pS to 1.1 nS in steps of 50 pS. a: measured potential responses (top) and conductance transients (bottom). b: peak membrane potential during each transient as a function of the K scaling value. Triangles: measured values. Solid line: computed responses for passive cell ($R = 3.79$ GΩ, C = 2.2 pF).

showed a much higher variation in spike amplitude when compared to injection of a single conductance transient eliciting the same maximum response (not shown), and the greatest variation was at the optimal separation.

Discussion

The accuracy of the present method depends upon sufficiently fast current injection by the current-clamp amplifier, such that the commanded current is not filtered significantly, and on the delay with which the current command is updated by the real-time computer, δt, which should be short enough not to give rise to aliasing of the voltage transient. The close agreement of the time course and amplitude of voltage transients with the calculated transients in the model cell (Fig. 2), implies that neither source of error was significant for passive responses to the synthetic synaptic conductance transients. In the neurons examined, the 17 kHz sampling rate used was sufficient not to alias measured active responses, and current-clamp showed a fast time constant of about 50 μs. However, for cells with much larger active currents, for example at a later stage of development, it would be important to use a conventional amplifier designed for high-speed current-clamp with a voltage follower at the input stage, instead of a patch-clamp amplifier, and also to decrease δt further to prevent aliasing of the sampled potential.

We used the product of 2 exponentials (Eqn. 2) to describe the form of synaptic conductance changes, and showed that such a function provides good fits to natural synaptic inhibitory and fast excitatory currents in these cells. When the ratio $\tau_1 : \tau_2$ is large, this function becomes close to the difference (or convolution) of 2 exponentials, which may be expected theoretically if transmitter release is effectively pulsatile and synaptic channels have a single open and a single closed state. However, the method permits any

form of conductance transient template to be used; indeed, natural synaptic currents recorded at a constant potential V and scaled down by a factor of $(E_{rev} - V)$, could be used directly as the conductance template.

The time course of the current injected during conductance injection can differ radically from that of the conductance transient, as seen in Fig. 3, owing to the dynamic sensitivity of the current to the potential. As expected, conductance injection gave the same saturating and reversible responses as do natural synaptic conductances (Figs. 3 and 4). It thus offers a considerably more realistic way to measure neuronal stimulus–response characteristics than does prescribed current injection. The relationship of K (peak conductance) to $V(t)$ showed significant non-linearity (Fig. 4), in the passive range of membrane potential as well as in the range of active responses.

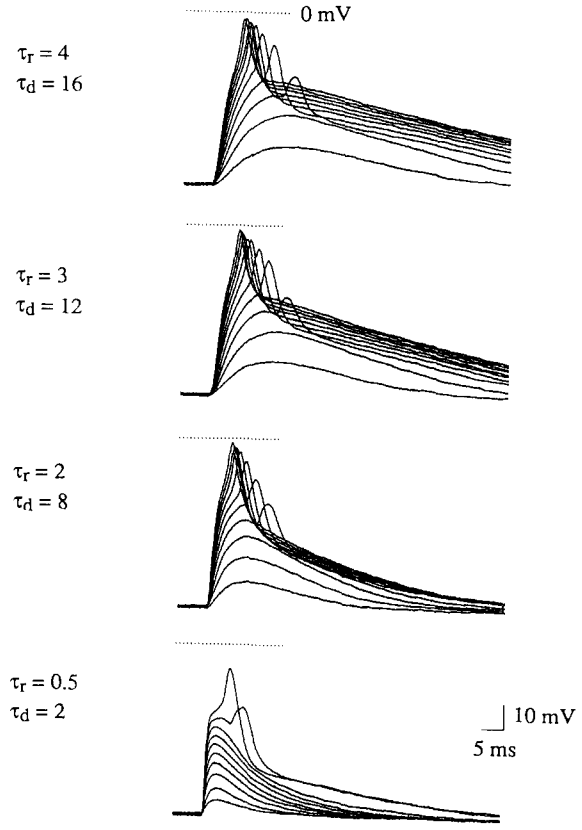

Fig. 5. Effect of variation of kinetics of transient conductance inputs. Families of conductance transients were injected as in Fig. 3. For each set of values of τ_1 and τ_2 (indicated on the left), K was stepped from 100 pS to 1 nS in increments of 100 pS.

Temporal summation of 2 excitatory conductance transients revealed an even greater non-linearity of response (Fig. 6), with a sharply defined optimum interval between transients for eliciting the maximum depolarization, in this case at about 5 ms. This phenomenon could lead to a resonant amplification of conductance inputs at a preferred frequency. The variability of the response even at the optimum interval could be explained if the second conductance transient occurs when the membrane has been brought close to a relatively non-linear state by the first transient. The second response would therefore become a sensitive function of the membrane potential reached, and would be highly susceptible to perturbation by membrane current noise.

We have demonstrated that conductance injection allows the functional role of synaptic conductances characterized by voltage-clamp to be studied directly and quantitatively in unclamped excitable cells, obviating a full reconstruction of the membrane currents by numerical modelling. The site of conductance injection is the site of the electrode, and simulation of remote dendritic synaptic conductance transients would require appropriate placement of the electrode. Specific chemical effects of ions such as Ca^{2+} flowing during natural conductance transients are not, of course, duplicated by the present method; this could, however, be useful in differentiating between chemically dependent and purely electrical components of synaptic responses. The technique could be extended in a number of ways. Using the much greater processing speeds of the presently available digital signal processor chips, it would be possible to measure the interaction of several time-dependent conductances with different reversal potentials, as in simultaneous excitatory and inhibitory synaptic input. One additional multiplication per δt with a value in a look-up table would enable simulation of permeabilities with non-linear instantaneous current-voltage relationships, such as the NMDA receptor channel (Mayer et al., 1984; Nowak et al., 1984). The injection of conductances with voltage-dependent

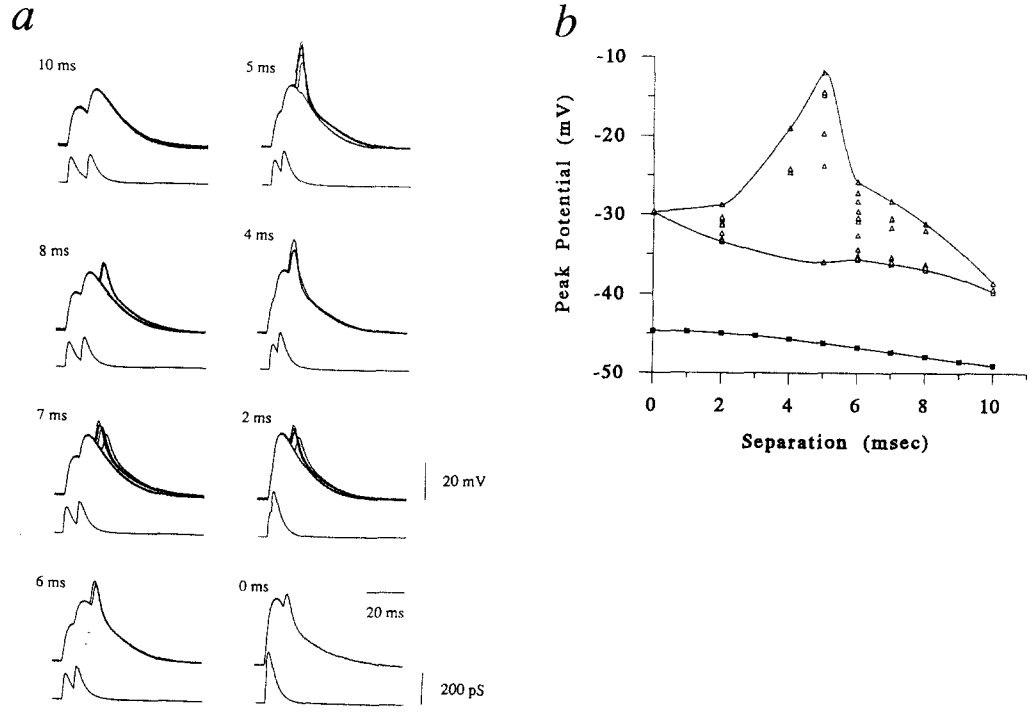

Fig. 6. Temporal summation of excitatory conductance inputs. a: the sum of 2 identical conductance transients ($K = 300$ pS, $\tau_1 = 1$ ms, $\tau_2 = 4$ ms, $E_{rev} = 0$ mV) offset by various intervals between 0 and 10 ms was injected into a neuron. Three to 10 records were acquired at each interval, with 10 s between trials. b: the peak membrane potential reached was plotted as a function of the separation between the summed conductance transients (open triangles). Solid lines indicate the envelope of the response, which showed a marked optimum at 5 ms separation between conductance transients. Filled squares: computed response of the passive circuit of the neuron.

kinetics described by the conventional model (Hodgkin and Huxley, 1952) would be feasible if the rate equations could be integrated accurately in real time. Injection of negative conductance could be used to cancel or titrate intrinsic conductances.

Acknowledgements

We thank Prof. Vincent Torre, Universitá di Genova, for his comments. This work was supported by a grant from the Japanese Ministry of Science and Culture, No. 63060006.

References

Barrett, J.N. and Crill, W.E. (1974) Influence of dendritic location and membrane properties on the effectiveness of synapses on cat motoneurones. J. Physiol., 239: 325–345.

Bekkers, J.M. and Stevens, C.F. (1989) NMDA and non-NMDA receptors are colocalized at individual excitatory synapses in cultured rat hippocampus. Nature, 341: 230–233.

Forsythe, I.D. and Westbrook, G.L. (1988) Slow excitatory postsynaptic currents mediated by *N*-methyl-D-aspartate receptors on cultured mouse central neurones. J. Physiol. (Lond.), 396: 515–533.

Hamill, O.P., Marty, A., Neher, E., Sakmann, B. and Sigworth, F.J. (1981) Improved patch-clamp techniques for high-resolution current recording from cells and cell-free membrane patches. Pflügers Arch., 391: 85–100.

Hestrin, S., Nicoll, R.A., Perkel, D.J. and Sah, P. (1990) Analysis of excitatory synaptic action in pyramidal cells using whole-cell recording from rat hippocampal slices. J. Physiol. (Lond.), 422: 203–225

Hodgkin, A.L. and Huxley, A.F. (1952) A quantitative description of membrane current and its application to conduction and excitation in nerve. J. Physiol. (Lond.), 117: 500–544.

Johansson, S., Friedman, W. and Århem, P. (1992) Impulses and resting membrane properties of small cultured rat hippocampal neurons, J. Physiol. (Lond.), 445: 129–140.

Llinás, R.R. (1988) The intrinsic electrophysiological properties of mammalian neurons: insights into central nervous system function. Science, 242: 1654–1664.

Keller, B.U., Konnerth, A. and Yaari, Y. (1991) Patch clamp analysis of excitatory synaptic currents in granule cells of rat hippocampus. J. Physiol. (Lond.), 435: 275–293.

Koch, C., Poggio, T. and Torre, V. (1983) Nonlinear interactions in a dendritic tree: localization, timing, and role in information processing. Proc. Natl. Acad. Sci. (USA), 80: 2799–2802.

MacGregor, R.J. (1968) A model for responses to activation by axodendritic synapses. Biophys. J., 8: 305–318.

Mayer, M.L., Westbrook, G.L. and Guthrie, P.B. (1984) Voltage-dependent block by Mg^{2+} of NMDA responses in spinal cord neurones. Nature, 309: 261–263.

Nowak, L., Bregestovski, P., Ascher, P., Herbet, A. and Prochiantz, A. (1984) Magnesium gates glutamate-activated channels in mouse central neurons. Nature, 307: 462–465.

Poggio, T. and Torre, V. (1978) A new approach to synaptic interactions. In: R. Heim and G. Palm (Eds.), Approaches to complex systems, Springer, Berlin, pp. 89–115.

Rall, W. (1977) Core conductor theory and cable properties of neurons. In: E.R. Kandel (Ed.), Handbook of Physiology, The Nervous System, Vol. 1, Section 1, Am. Physiol. Soc., Bethesda, MD.

Robinson, H.P.C. (1991) Kinetics of synaptic conductances in mammalian central neurons. Neurosci. Res., Suppl. 16: VI.

Robinson, H.P.C., Sahara, Y. and Kawai, N. (1991) Nonstationary fluctuation analysis and direct resolution of single channel currents at postsynaptic sites. Biophys. J., 59: 295–304.

Segal, M. and Barker, J.L. (1984) Rat hippocampal neurons in culture: voltage-clamp analysis of inhibitory synaptic connections. J. Neurophysiol., 52: 469–487.

Shirasaki, T., Klee, M.R., Nakaye, T. and Akaike, N. (1991) Differential blockade of bicuculline and strychnine on GABA- and glycine-induced responses in dissociated rat hippocampal pyramidal cells. Brain Res., 561: 77–83.

Tuckwell, H.C. (1988) Introduction to Theoretical Neurobiology, Vol. 2, Nonlinear and Stochastic Theories, Cambridge University Press, Cambridge, UK, 265 pp.

Turner, D.A. (1984) Conductance transients onto dendritic spines in a segmental cable model of hippocampal neurons. Biophys. J., 46: 85–96.

Wathey, J.C., Lytton, W.W., Jester, J.M. and Sejnowski, T.J. (1992) Computer simulations of EPSP-spike (E-S) potentiation in hippocampal CA1 pyramidal cells. J. Neurosci., 12: 607–618.

JOURNAL OF NEUROPHYSIOLOGY
Vol. 69, No. 3, March 1993. *Printed in U.S.A.*

RAPID PUBLICATION

Dynamic Clamp: Computer-Generated Conductances in Real Neurons

ANDREW A. SHARP, MICHAEL B. O'NEIL, L. F. ABBOTT, AND EVE MARDER
Departments of Biology and Physics, and Center for Complex Systems, Brandeis University, Waltham, Massachusetts 02254

SUMMARY AND CONCLUSIONS

1. We describe a new method, the dynamic clamp, that uses a computer as an interactive tool to introduce simulated voltage and ligand mediated conductances into real neurons.

2. We simulate a γ-aminobutyric acid (GABA) response of a cultured stomatogastric ganglion neuron to illustrate that the dynamic clamp effectively introduces a conductance into the target neuron.

3. To demonstrate an artificial voltage-dependent conductance, we simulate the action of a voltage-dependent proctolin response on a neuron in the intact stomatogastric ganglion. We show that shifts in the activation curve and the maximal conductance of the response produce different effects on the target neuron.

4. The dynamic clamp is used to construct reciprocal inhibitory synapses between two stomatogastric ganglion neurons that are not coupled naturally, illustrating that this method can be used to form new networks at will.

INTRODUCTION

The electrical activity of a system of interacting neurons arises from a complex dynamic interplay between numerous voltage and ligand mediated conductances (Harris-Warrick and Marder 1991). Remarkable progress has been made in describing the properties of individual membrane conductances by using voltage and patch-clamp methods (Hille 1992). However, these methods do not provide a direct understanding of the role each conductance plays in shaping the electrical activity of a neuron or network. Pharmacological agents can be used to block individual currents to assess their role in neuronal behavior (Calabrese and DeSchutter 1992; Meer and Buchanan 1992; Tierney and Harris-Warrick 1992), but lack of specificity or lack of availability of appropriate blockers limits the utility of this method. An alternate approach, computer simulation, (Koch and Segev 1989; Marder and Selverston 1992; Traub et al. 1992) is limited by the difficulty of accurately measuring all of the currents found in all of the neurons in a biological network. Moreover, the strengths of synapses in biological networks are often difficult, if not impossible, to measure. The dynamic clamp described here offers a third and novel solution to this problem. Investigator-specified conductances are added to individual neurons or used to create artificial synapses, allowing the study of these conductances and synapses in functioning networks.

METHODS

Recordings

Cancer borealis were purchased from local (Boston, MA) fishermen. Experiments on intact stomatogastric ganglia (STGs) were done as described in Weimann et al. (1991). Experiments on cultured neurons were done as described in Sharp et al. (1992). Physiological saline had the following composition (in mM): 440 NaCl, 11 KCl, 13 $CaCl_2$, 26 $MgCl_2$, pH 7.45. Recordings were made with single intracellular electrodes filled with 0.6 M K_2SO_4 and 20 mM KCl. The recording amplifiers (Axoclamp-2A) were used in discontinuous current clamp mode with a sampling rate of 5 kHz.

Current calculation

A membrane current (I) to be applied to a neuron is given by $I = gm^p h^q(V - E_r)$ where p and q are integers, E_r is the reversal potential of the current, and V is membrane potential. The activation and inactivation variables (Hille 1992; Hodgkin and Huxley 1952) are described by first order, nonlinear differential equations

$$\tau_m(V)\frac{dm}{dt} = m_\infty(V) - m \qquad \tau_h(V)\frac{dh}{dt} = h_\infty(V) - h$$

where τ_m, τ_h, m_∞, and h_∞ are functions of V.

Synaptic conductance

To construct a synapse we use the membrane potential of the presynaptic neuron (V_{pre}) to control the conductance of the postsynaptic neuron. The synaptic current is given by

$$I = gs(E_r - V_{post})$$

where E_r is the synaptic reversal potential and V_{post} the membrane potential of the postsynaptic neuron. The synaptic activation variable s varies between zero and one and is determined by

$$(1 - s_\infty(V_{pre}))\tau_s\frac{ds}{dt} = s_\infty(V_{pre}) - s$$

where s_∞ is given as a function of the presynaptic potential by

$$s_\infty(V_{pre}) = \tanh[(V_{pre} - V_{th})/\Delta]$$

for presynaptic potentials V_{pre} satisfying $V_{pre} > V_{th}$, otherwise $s_\infty = 0$. V_{th} and Δ are constants.

RESULTS

Artificial conductances

The properties of membrane conductances can be described by differential equations that relate the opening and closing of membrane channels to membrane potential and time. The current flowing through a given conductance can be computed if one knows the membrane potential and the reversal potential for the conductance. The dynamic clamp uses a computer to control the current injected through a microelectrode into a cell as a function of the membrane potential of the cell and properties of the conductance speci-

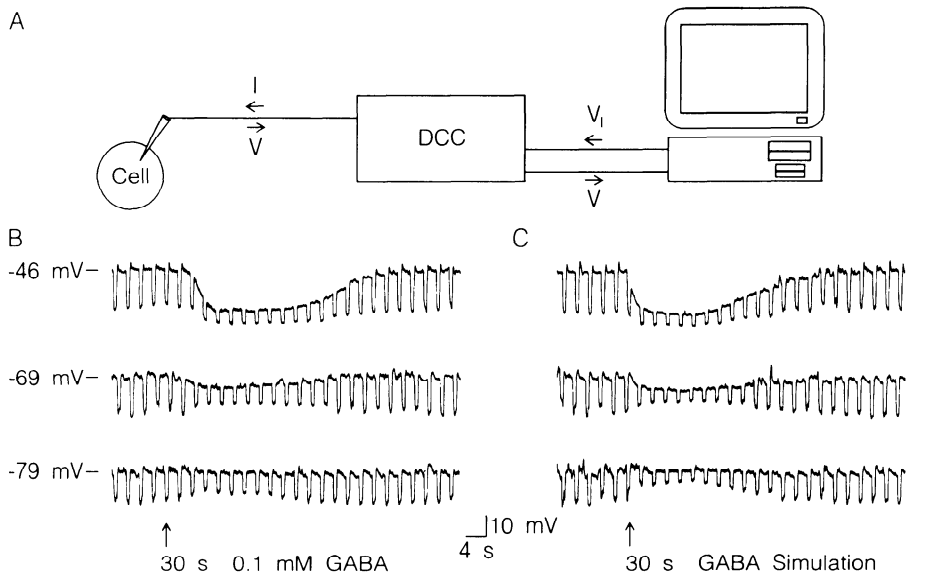

FIG. 1. Dynamic clamp. *A*: schematic of the dynamic clamp. *B*: intracellular recording from a neuron in primary cell culture dissociated from the stomatogastric ganglion (STG) of the crab, *Cancer borealis* (Sharp et al. 1992). Constant hyperpolarizing pulses (−0.05 nA) were applied every 3 s. At the upward arrow, the continuously flowing superfusion solution was changed for 30 s from control saline to 10^{-4} M γ-aminobutyric acid (GABA). This procedure was repeated at the different potentials shown. *C*: same as *B*, but the dynamic clamp was programmed to simulate a conductance change of 8 nS with a reversal potential of −75 mV. The conductance had an exponential rise (τ = 5 s) and fall (τ = 15 s).

fied by the investigator. The membrane potential of a dynamically clamped neuron is measured with intracellular electrodes by an Axoclamp 2A in discontinuous current-clamp mode (Fig. 1*A*). *V* is transmitted to the computer through an analog-to-digital converter. On the basis of *V* and differential equations describing a model conductance programmed into the computer, *I* is computed. This is converted back into an analog voltage (V_I) and transmitted to

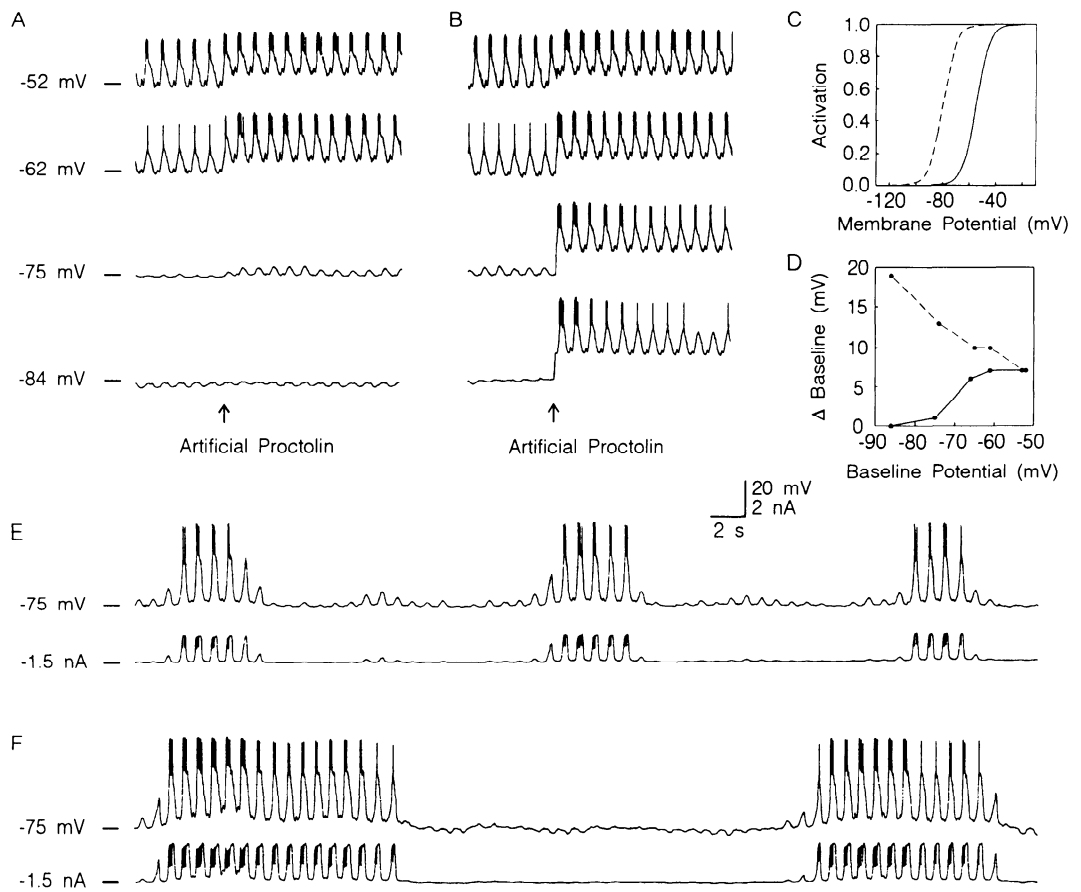

FIG. 2. Artificial proctolin response. *A*: intracellular recordings from an inferior cardiac (IC) neuron in the stomatogastric ganglion (STG) at the potentials indicated. The artificial proctolin conductance was turned on at the upward arrow (g = 40 nS, E_r = −10 mV, τ_m = 6 ms). The activation curve for the proctolin current is the solid line in *C*. *B*: same as *A*, but the activation curve is the dashed line in *C*. *D*: plot of the amplitude of the proctolin response as a function of *V*, for the activation curve used in *A* (——) and that used in *B* (- - -). *E*: *top* is membrane potential; *bottom* is injected current. The neuron is hyperpolarized by the same amount as in the third trace of *A*. The proctolin conductance was 60 nS; other parameters are as in *A*. *F*: same as *E* except g = 90 nS.

the Axoclamp which injects the computed current into the neuron. By adjusting the parameters of the computer-implemented conductance, we control the characteristics (e.g., activation threshold, time constant, and reversal potential) of the simulated conductance.

Because the current injected by the dynamic clamp at any moment depends on the membrane potential measured at that time, this technique effectively changes the conductance of the neuron, and mimics the effects of opening real membrane channels, as illustrated in Fig. 1, *B* and *C*. In both panels, pulses of constant current were applied to a neuron to monitor its input resistance. 10^{-4} M GABA (γ-aminobutyric acid) was applied at the time indicated by the arrow in Fig. 1*B*, resulting in an increase in conductance. The GABA response was hyperpolarizing at −46 mV and showed a reversal potential of ~ −80 mV. Figure 1*C* shows the use of the dynamic clamp to mimic the GABA-activated conductance. As with the GABA application, the dynamic clamp increases the effective conductance and produces changes in membrane potential that depend on the driving force.

Some ligand-gated conductances are voltage dependent. Figure 2 illustrates the use of the dynamic clamp to simulate the voltage-dependent effect of the peptide proctolin (Golowasch and Marder 1992) on the inferior cardiac neuron (IC) of the crab STG by using the equations used in previous modeling studies (Buchholtz et al. 1992; Golowasch et al. 1992). Figure 2*A* shows the IC neuron at four different levels of steady-state current injection. The simulated proctolin conductance was applied at the upward arrow in each of the traces. Because of the voltage dependence of the proctolin conductance, this produces a substantial depolarization of the membrane potential when the neuron is at depolarized levels but relatively little effect at more hyperpolarized levels (Fig. 2*D*). If the activation threshold of the simulated proctolin conductance is changed (Fig. 2, *B* and *C*), the proctolin activated conductance now produces a depolarization throughout the voltage range illustrated (Fig. 2, *B* and *D*).

Complex phenomena can result from the interaction of a voltage-dependent noninactivating conductance (such as the proctolin conductance) with other membrane conductances (Fig. 2, *E* and *F*). The recordings in Fig. 2, *E* and *F* are at the same baseline membrane potential as trace 3 of Fig. 2*A*. In response to increasing the proctolin conductance from 40 to 60 nS (Fig. 2*E*), the cell produced periodic bouts of bursting behavior. When the proctolin conductance was further increased to 90 nS (Fig. 2*F*), the burst duration increased. The voltage dependence of the proctolin conductance is crucial for this behavior; it cannot be produced simply by depolarizing the neuron with continuous current injection (not shown). Note that increasing the proctolin current by increasing the maximal conductance produced very different effects than those produced by a negative shift in the activation curve (Fig. 2*B*).

Artificial synapses

The dynamic clamp can be used to create artificial chemical synapses between two neurons. Figure 3*A* illustrates the procedure. When the presynaptic potential crosses the threshold potential (V_{th}) the postsynaptic conductance is calculated as a function of the presynaptic potential and a deactivation time constant. The current injected into a follower neuron is the product of the conductance and a driving force that is the difference between the potential of the postsynaptic neuron and a reversal potential. Figure 3*B* shows artificial inhibitory postsynaptic potentials (IPSPs) evoked in a follower neuron at different membrane potentials and illustrates the effect of changing the reversal potential of the programmed IPSP.

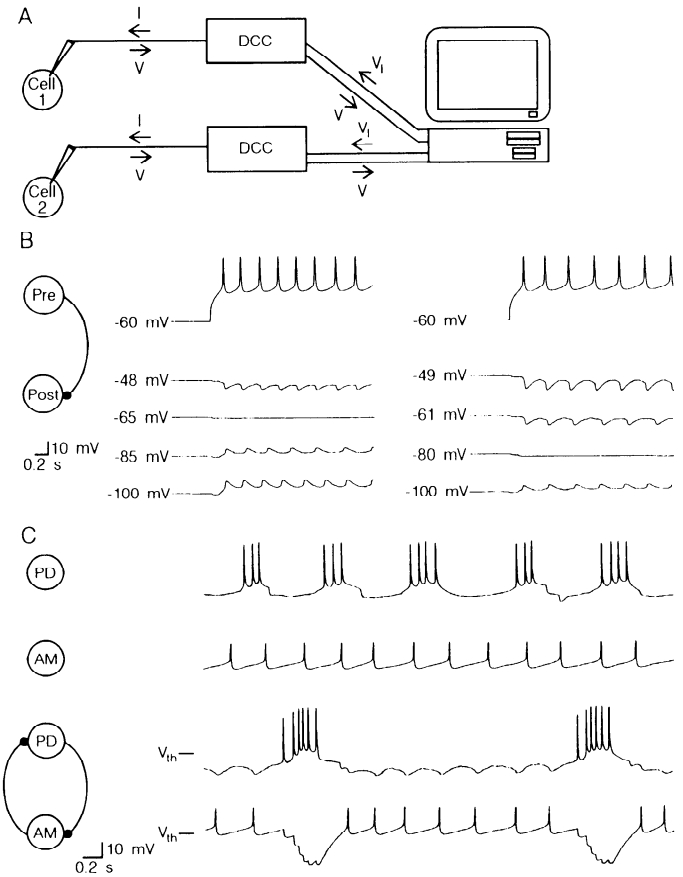

FIG. 3. Artificial chemical synapses. *A*: schematic showing the use of the dynamic clamp to construct artificial synapses. *B*: simultaneous intracellular recordings from two stomatogastric ganglion (STG) neurons. *Top*: action potentials in the presynaptic neuron evoked by depolarization; *bottom* artificial inhibitory postsynaptic potentials (IPSPs) in the postsynaptic neuron at the potentials indicated evoked by action potentials in the presynaptic neuron. *Left*: E_r is −65 mV; *right*: E_r is −80 mV. *C*: simultaneous intracellular recordings from a Pyloric Dilator (PD) neuron and an Anterior Median (AM) neuron in the STG. Under control conditions (*top*) these neurons show no synaptic interactions. *Bottom*: reciprocal inhibition established between these neurons by using the dynamic clamp (V_{th} for PD = −45 mV, V_{th} for AM = −30 mV, and for both neurons g = 100 nS, E_r = −80 mV, and Δ = 40 mV).

In Fig. 3*C*, two neurons from the stomatogastric ganglion, unconnected in the control condition, were connected with artificial reciprocal inhibitory synapses. Note that the new synaptic connections result in a change in the frequency and intensity of the bursts as an emergent property of the new network.

DISCUSSION

Because the dynamic clamp creates an artificial conductance rather than injecting current (Yarom 1991), it repli-

cates accurately the way in which a current interacts with others in the cell and makes possible an array of experiments not feasible heretofore. It allows the investigator to explore, with real neurons, the role of ionic currents in shaping neuronal firing patterns. Physiological applications of modulators, such as proctolin, often result in complex changes in neural networks (Heinzel and Selverston 1988; Hooper and Marder 1987; Marder 1991). We now can ask which of those changes are a direct consequence of a single modulatory current and which may involve multiple sites of action within the network.

By using the dynamic clamp, the accuracy with which a given conductance can be simulated is equivalent to the accuracy with which the current can be measured and modeled. The utility of this method in each preparation will depend on the speed of the currents and whether there are appreciable cable effects. In many neurons the currents of interest are relatively slow, in particular those that perform modulatory roles. The dynamic clamp is particularly well suited for the analysis of these currents. Although not described at length here, the dynamic clamp can also be used, with certain limitations, to "subtract" the effect of an existing conductance in a neuron thus acting as an electronic "blocker" or "antagonist."

Analog circuits have been used previously to create artificial electrical synapses (Joyner et al. 1991; Sharp et al. 1992). We can now also form circuits with artificial chemical synapses among cultured neurons without relying on the fortuitous formation of naturally occurring synapses (Kleinfeld et al. 1990; Lukowiak 1991; Syed et al. 1990). We can modify circuits in ganglia by adding synaptic connections where they are not present. Finally, we can connect real time computer model neurons to biological neurons (LeMasson et al. 1992). The dynamic clamp makes tangible the interactions between theory and experimental work in neuroscience and should allow the exploration of the many aspects of dynamic network function not previously possible.

We thank Dr. John Rinzel for early discussions and J. McCarthy for help with manuscript preparation.

This research was supported by BNS9009251 from the National Science Foundation and MH-46742 from the National Institutes of Mental Health.

Address reprint requests to E. Marder.

Received 3 December 1992; accepted in final form 8 December 1992.

REFERENCES

BUCHHOLTZ, F., GOLOWASCH, J., EPSTEIN, I. R., AND MARDER, E. Mathematical model of an identified stomatogastric ganglion neuron. *J. Neurophysiol.* 67: 332–340, 1992.

CALABRESE, R. AND DESCHUTTER, E. Motor pattern generating networks in invertebrates: modeling our way toward understanding. *Trends Neurosci.* 15: 439–445, 1992.

GOLOWASCH, J., BUCHHOLTZ, F., EPSTEIN, I. R., AND MARDER, E. Contribution of individual ionic currents to activity of a model stomatogastric ganglion neuron. *J. Neurophysiol.* 67: 341–349, 1992.

GOLOWASCH, J. AND MARDER, E. Proctolin activates an inward current whose voltage-dependence is modified by extracellular Ca^{++}. *J. Neurosci.* 12: 810–817, 1992.

HARRIS-WARRICK, R. M. AND MARDER, E. Modulation of neural networks for behavior. *Annu. Rev. Neurosci.* 14: 39–57, 1991.

HEINZEL, H. G. AND SELVERSTON, A. I. Gastric mill activity in the lobster. III. The effects of proctolin on the isolated central pattern generator. *J. Neurophysiol.* 59: 566–585, 1988.

HILLE, B. *Ionic Channels of Excitable Membranes* (2nd ed.). Sunderland, MA: Sinauer, 1992.

HODGKIN, A. L. AND HUXLEY, A. F. A quantitative description of membrane current and its application to conduction and excitation in nerve. *J. Physiol.* 117: 500–544, 1952.

HOOPER, S. L. AND MARDER, E. Modulation of the lobster pyloric rhythm by the peptide proctolin. *J. Neurosci.* 7: 2097–2112, 1987.

JOYNER, R. W., SUGIWARA, H., AND TAU, R. C. Unidirectional block between isolated rabbit ventricular cells coupled by a variable resistance. *Biophys. J.* 60: 1038–1045, 1991.

KLEINFELD, D., RACCVIA-BEHLING, F., AND CHIEL, H. J. Circuits constructed from identified *Aplysia* neurons exhibit multiple patterns of persistent activity. *Biophys. J.* 57: 697–715, 1990.

KOCH, C. AND SEGEV, I. *Methods in Neuronal Modeling.* Cambridge, MA: MIT Press, 1989.

LEMASSON, G., RENAUD-LEMASSON, S., SHARP, A., ABBOTT, L. F., AND MARDER, E. Real time interaction between a model neuron and the crustacean stomatogastric nervous system. *Soc. Neurosci. Abstr.* 18: 1055, 1992.

LUKOWIAK, K. Experimental reconstruction of neuronal pattern generators. *Curr. Opin. Neurobiol.* 1: 577–582, 1991.

MARDER, E. Modifiability of pattern generation. *Curr. Opin. Neurobiol.* 1: 571–576, 1991.

MARDER, E. AND SELVERSTON, A. I. Modelling the Stomatogastric Nervous System. In: *Dynamic Biological Networks: The Stomatogastric Nervous System,* edited by R. M. Harris-Warrick, E. Marder, A. I. Selverston, and M. Moulins. Cambridge, MA: MIT Press, 1992.

MEER, D. P. AND BUCHANAN, J. T. Apamin reduces the late afterhyperpolarization of lamprey spinal neurons, with little effect on fictive swimming. *Neurosci. Lett.* 143: 1–4, 1992.

SHARP, A. A., ABBOTT, L. F., AND MARDER, E. Artificial electrical synapses in oscillatory networks. *J. Neurophysiol.* 67: 1691–1694, 1992.

SYED, N. I., BULLOCH, A. G. M., AND LUKOWIAK, K. In vitro reconstruction of the respiratory central pattern generator of the mollusk *Lymnaea. Science Wash. DC* 250: 282–285, 1990.

TIERNEY, A. J. AND HARRIS-WARRICK, R. M. Physiological role of the transient potassium current in the pyloric circuit of the lobster stomatogastric ganglion. *J. Neurophysiol.* 67: 599–609, 1992.

TRAUB, R. D., WONG, R. K. S., MILES, R., AND MICHELSON, H. A model of a CA3 hippocampal pyramidal neuron incorporating voltage-clamp data on intrinsic conductances. *J. Neurophysiol.* 66: 635–650, 1992.

WEIMANN, J. M., MEYRAND, P., AND MARDER, E. Neurons that form multiple pattern generators: identification and multiple activity patterns of gastric/pyloric neurons in the crab stomatogastric system. *J. Neurophysiol.* 65: 111–122, 1991.

YAROM, Y. Rhythmogenesis in a hybrid system interconnecting an olivary neuron to an analog network of coupled oscillators. *Neurosci.* 44: 263–275, 1991.

Interacting biological and electronic neurons generate realistic oscillatory rhythms

Attila Szűcs,[CA] Pablo Varona, Alexander R. Volkovskii, Henry D. I. Abarbanel,[1] Mikhail I. Rabinovich and Allen I. Selverston

Institute for Nonlinear Science, University of California San Diego, 9500 Gilman Drive, La Jolla, CA 92093-0402; [1]Department of Physics and Marine Physical Laboratory, Scripps Institution of Oceanography, University of California San Diego, La Jolla, CA 92093-0402, USA

[CA]Corresponding Author

Received 22 October 1999; accepted 9 December 1999

Acknowledgements: Partial support for this work comes from the US Department of Energy, Office of Basic Energy Sciences, Division of Engineering and Geosciences, under grant DE-FG03-90ER14138 and DE-FG03-96ER14592.

Small assemblies of neurons such as central pattern generators (CPG) are known to express regular oscillatory firing patterns comprising bursts of action potentials. In contrast, individual CPG neurons isolated from the remainder of the network can generate irregular firing patterns. In our study of cooperative behavior in CPGs we developed an analog electronic neuron (EN) that reproduces firing patterns observed in lobster pyloric CPG neurons. Using a tuneable artificial synapse we connected the EN bidirectionally to neurons of this CPG. We found that the periodic bursting oscillation of this mixed assembly depends on the strength and sign of the electrical coupling. Working with identified, isolated pyloric CPG neurons whose network rhythms were impaired, the EN/biological network restored the characteristic CPG rhythm both when the EN oscillations are regular and when they are irregular. *NeuroReport* 11:563–569 © 2000 Lippincott Williams & Wilkins.

Key words: Electronic neuron; Electronic synapse; Oscillatory rhythm; Pyloric neurons; Regularization; Synchronization

INTRODUCTION

Central pattern generators (CPGs) are widely studied systems of rhythm generation in small neuron assemblies [1]. The regularity and stationarity of the oscillatory patterns generated by a small number of interacting neurons is noteworthy, especially in light of evidence that such networks are composed of individual neurons which can oscillate chaotically when observed in isolation. Indeed, CPG neurons with their synaptic inputs blocked have been shown to express chaotic firing patterns [2–6]. Regular rhythm generating neurons called pacemakers are commonly believed to be fundamental parts of the CPGs, initiating the main oscillation [7]. A pacemaker neuron or group may be required to synchronize all other neurons and control joint rhythms because of the differences in the properties of individual neurons.

The stomatogastric ganglion (STG) of crustaceans is a well understood nervous system [8]. It contains the pyloric CPG that generates a highly regular and repetitive motor pattern resulting from interactions between 14 neurons. In this system the anterior burster (AB) neuron is one of the main pacemaker elements, having a central role in organizing the rhythm. The two electrically coupled pyloric dilator (PD) neurons fire in-phase with the AB forming a triplet of pacemaker neurons. The robustness and uniformity of the oscillation initiated by AB makes it difficult to manipulate or interact with the rhythm and investigate the role of individually irregular PDs in the pattern generation.

Based on our non-linear analysis of experimental data from isolated pyloric neurons, we have developed a simple analog electronic model of CPG neurons capable of reproducing the observed firing patterns. The 'electronic neuron' (EN) was connected to the PD cells using an artificial synapse, thus forming a mixed circuit. This approach allowed us to dynamically interact with the biological neurons rather than stimulating them using response-independent current commands. In this fashion we have shown that the regular, natural rhythm of the PD in the intact network is restored when interacting with the ENs. This occurs both when the EN is behaving regularly and when it is set into a state of chaotic oscillations.

MATERIALS AND METHODS

Preparation and electrophysiology: The stomatogastric nervous system (STNS) of the spiny lobster *Panulirus interruptus* L. was dissected and prepared as described earlier [9]. Briefly, the STG, the oesophageal ganglion and the two comissural ganglia with the interconnecting nerves were separated from the stomach and pinned in a Sylgard-lined Petri dish containing standard *Panulirus* physiologi-

cal saline [3]. The STG was perfused separately from the rest of the STNS using a vaseline chamber. Picrotoxin (PTX; 7.5 μM) was used to block glutamatergic synaptic transmission and isolating the pyloric pacemaker group from other pyloric neurons. Nerve cells were identified by comparing intracellular signals with extracellular burst patterns monitored simultaneously from output motor nerves. Partial isolation of the two PD neurons was performed by photoinactivating the presynaptic AB neuron [10]. The membrane potential of the cells was measured with Neuroprobe 1600 current-clamp amplifiers (AM-Systems). The PD neuron which we connected to the electronic neuron was impaled with two microelelectrodes filled with 3 M KCl and with resistances of 10-15 MΩ. One of these was used to monitor the membrane potential, while the other served as a current passing electrode. This method allowed us to avoid any problems arising from imperfect bridge balancing or non-linearities of the current passing electrode. A total of 198 trials were performed on nine preparations.

Electronic neuron and synapse: We have designed and built a three degree of freedom analog electronic circuit realization of a mathematical model of bursting neurons. The model was suggested by the work of Hindmarsh and Rose [11]. It uses a polynomial representation of the dependence of ion currents on the membrane potential according to the following differential equations:

$$\dot{x} = 4y + \frac{3x^2}{2} - \frac{x^3}{4} - 2z + \varepsilon, \qquad \dot{y} = \frac{1}{2} - \frac{5x^2}{8} - y,$$

$$\dot{z} = \mu(-z + 2x + 6.4)$$

where x is the membrane potential, y and z are 'fast' and 'slow' internal variables, ε represents the external currents, and μ is the time constant of the slow variable. Both ε and μ are tuneable parameters. The HR model captures the most important firing/bursting modes of real CPG neurons [12]. This model, however, generates spikes with too large an amplitude relative to the depth of interburst hyperpolarization. To make this ratio more realistic we used an additional nonlinear amplifier which reshaped the output of the HR model neuron and made the membrane potential oscillation more similar to that of bursting pyloric neurons (compare Fig. 1A, PD trace with Fig. 2A, EN trace). The EN, connected bidirectionally to the PD, was able to receive and process incoming signals in the same fashion as biological neurons receiving synaptic inputs. This functionality came from an additional electronic circuit simulating an electrotonic synapse. The potential difference between the EN and the biological neuron was measured, and a current signal proportional to the difference was generated. This current was fed back to the EN and connected to the current input of the intracellular amplifier with opposite polarity. The amplitude and sign of the current depended on the actual potential difference and a conductance parameter, set by the experimenter.

Data acquisition and analysis: The extra- and intracellular signals were acquired at 10 kS/s rate by the Axoscope 7.0 program running on a PC. Raw membrane potential data were visually inspected, and detailed quantitative analysis was performed using spike arrival times. The time derivative of the intracellular time series was used to detect spike events, and interspike-interval (ISI) sequences were constructed for each train. First-order return maps of the ISIs were used as a graphical tool characterizing the overall dynamics and the regularity of the firing patterns. The spike-density function (SDF) [13] was used to characterize modulations of the firing patterns and to detect correlations between simultaneous spike trains. The SDF technique allowed us to obtain firing rate as a continuous function of the elapsed time [14]. An SDF was constructed by convolving the time of each spike event with a Gaussian-function (kernel) of unit area and fixed half-width, typically 0.2 s here. The Fourier transform of the spike density functions was used to detect any periodicities

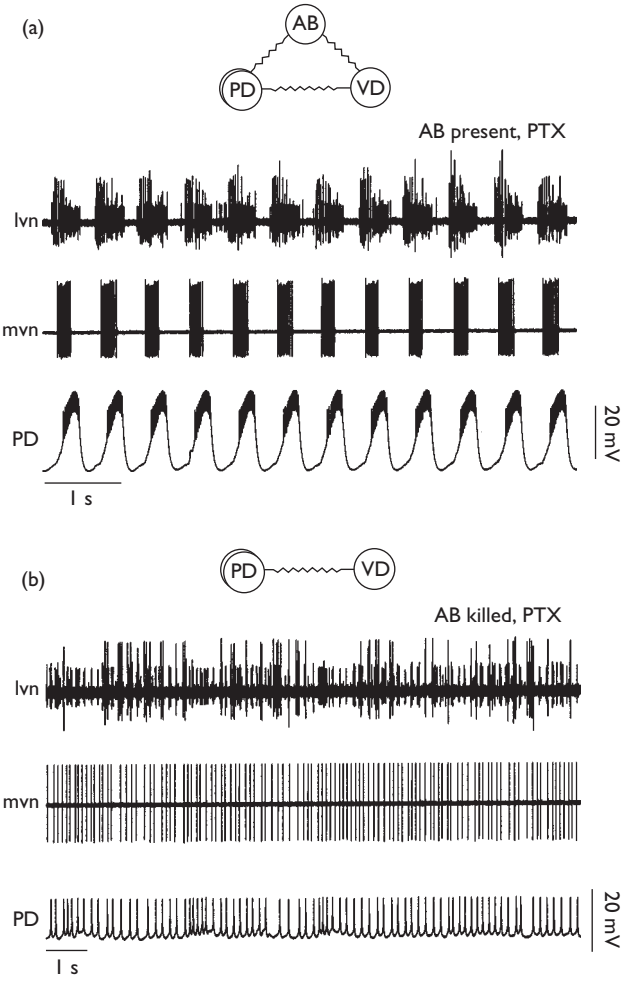

Fig. 1. Comparison of the activity patterns of pyloric neurons with the main pacemaker neuron AB present and shortly after photoinactivation of AB. Glutamatergic transmission was blocked by PTX. (**a**) Spikes of the LP (large), PD and PY (small) neurons appear in the extracellular recording from the lateral ventricular nerve (lvn). Activity of the VD neuron was monitored from the medial ventricular nerve (mvn). The bottom trace shows the firing pattern of the PD neuron (intracellular). (**b**) Disruption of the pyloric oscillation shortly after killing the AB neuron. PD and VD neurons were firing tonically; large spikes in the lvn recording indicate irregular bursts in LP.

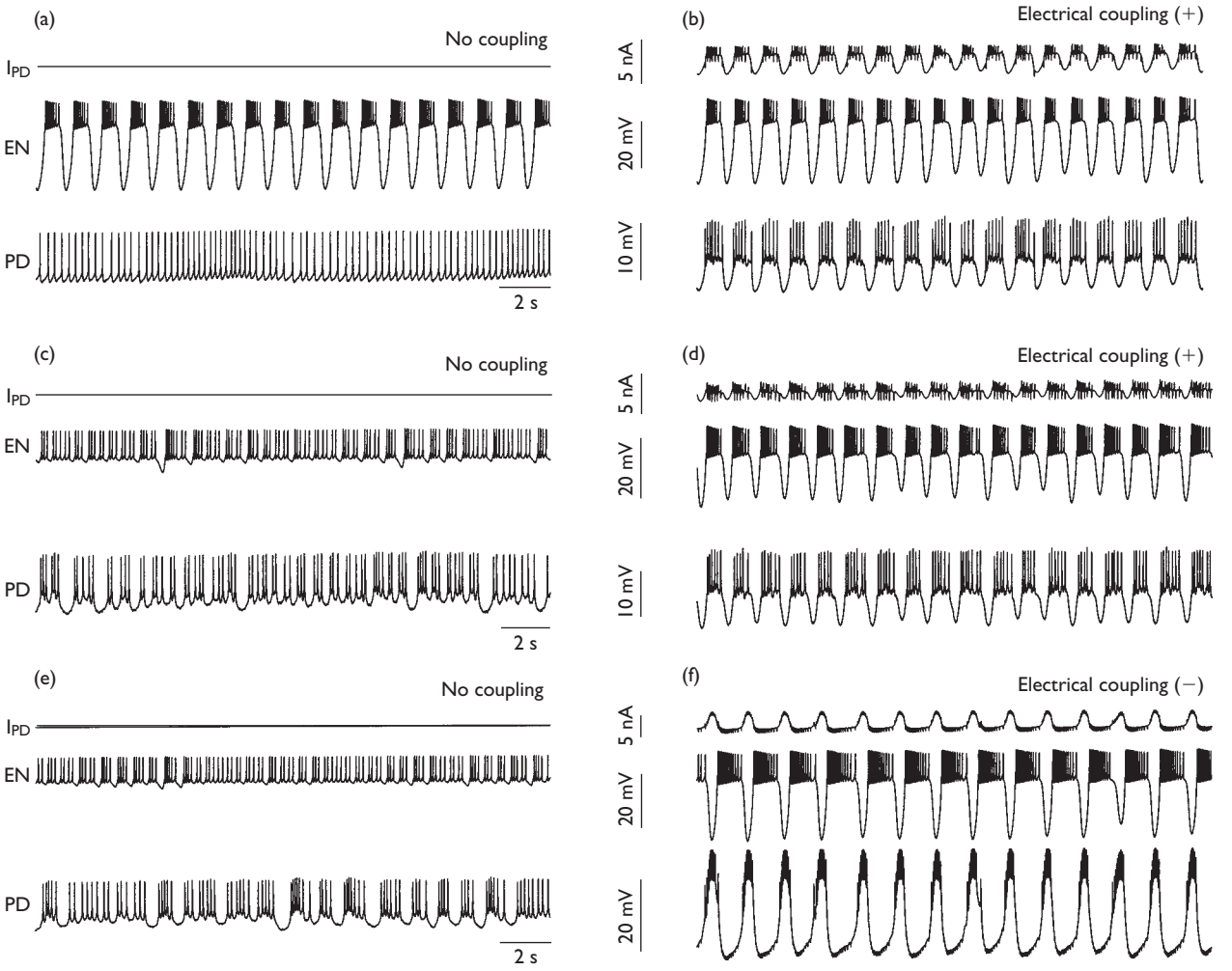

Fig. 2. Comparison of the intracellular firing patterns of the EN and the PD. Left panels: neurons disconnected, synapse off; right panels: electrotonic coupling. I_{PD} in each panel is the current flowing into PD through the electronic synapse. (**a**) Periodic bursting in EN with tonic spiking in PD (AB killed). (**b**) Synchronous bursting in EN and PD after switching on the electrical connection. (**c**) Chaotic firing in EN with irregular spiking in PD, no coupling. (**d**) Generation of the bursting pattern in the EN–PD mixed network after coupling via an electrotonic synapse. (**e**) Same as in (**c**). (**f**) Periodic antiphase bursting in EN and PD neuron with negative conductance connection.

in the firing patterns. Phase portraits were constructed by plotting the SDF of one neuron against that of the other. This graphical tool revealed cross-correlations between neurons recorded simultaneously.

RESULTS

Intact and reduced pyloric network: The pyloric pacemaker group of the lobster consists of four electrotonically coupled neurons: AB, two PDs and the VD neuron [7]. There are strong symmetrical connections between AB and the PD neurons and weaker rectifying connections between the AB and VD [15]. These nerve cells express a regular oscillatory pattern in the intact preparation (Fig. 1A). Picrotoxin, while blocking all glutamatergic synaptic inputs and functionally isolating the pacemaker network, had little effect on the frequency or amplitude of the ongoing oscillation. In contrast, photoinactivation of the main pacemaker neuron AB led to complete disruption of the pyloric rhythm. Removal of AB led to cessation of the bursting activity in PD neurons and in VD (Fig. 1B). Initially, after photoinactivation the PD expressed irregular spiking behavior that evolved after about 1 h into irregular bursting. The irregular bursting pattern remained for the lifetime of the preparation.

Connecting EN to isolated PD neurons—regular bursting: Because of the flexibility of our analog circuit, we could generate a broad range of firing/bursting patterns in EN by tuning the ε and μ parameters. In the experiments reported here, we first generated regular bursting in the EN and connected it to the PD. Essentially the EN behaved as a new pacemaker neuron: it acted as a replacement for the AB in the network. Prior to connection, we adjusted the parameters of the EN to obtain oscillation similar in amplitude (30–40 mV) and frequency (1.2–1.8 Hz) to that seen in AB. Electrotonic coupling shifted the firing pattern of PD from tonic spiking to bursting (Fig. 2A,B). The slow-wave components of the oscillations synchronized, while

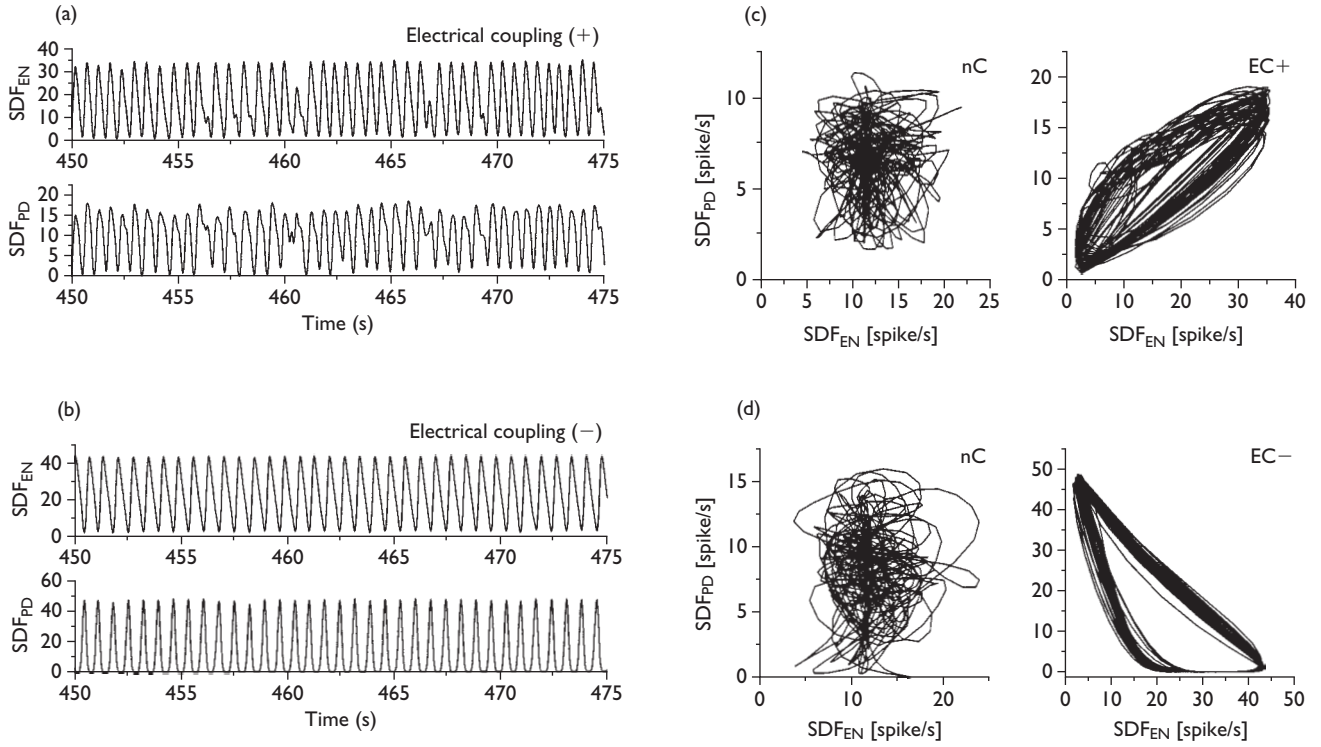

Fig. 3. Spike density functions (SDFs) calculated from the spike trains of coupled EN and PD neurons. (**a**,**b**) 25 s long sections of the SDFs with positive and negative conductance synaptic connections, respectively. The functions exhibit oscillating firing patterns in both neurons. Variation of the SDF is smaller when using negative conductance coupling, indicating strong mutual regularization. (**c**) Phase-portrait graphs before (nC, no connection) and after (EC+) connecting the EN to PD via positive conductance synapse. (**d**) Same graphs with negative conductance (EC−) connection.

single spikes in EN and PD did not. The bursting pattern of PD induced by the electrotonic coupling resembled that in the intact pyloric pacemaker network. Monitoring activity of the output nerve lvn showed that the burst pattern of the postsynaptic neuron LP was also synchronized with the EN–PD pair, leading to a partial restoration of the pyloric rhythm. Inserting EN as a regular, periodic bursting element into the impaired neuronal network induced a new overall oscillation, quite similar to the original pyloric rhythm.

Connecting chaotic electronic and pyloric neurons: The EN is also able to generate chaotic patterns. In this case, no periodic spike patterns were produced by the EN. Figure 2C shows the similarities of the time series of chaotic EN and the isolated PD neurons before coupling, both firing in an irregular manner. Non-linear analysis using the method of false nearest neighbors [16] of the bursting pattern of the free-running PD neuron indicated high-dimensional (up to seven) chaotic dynamics. Remarkably, electrotonic coupling dramatically altered the firing patterns of both EN and PD. Synchronized bursting appeared immediately after coupling the electronic model to the pyloric cell (Fig. 2D). The frequency of the bursting was close to that seen in the intact pyloric network. As a consequence of this high-degree of synchronization, the synaptic current being injected into PD showed only minor fluctuations.

To approximate a graded inhibitory synapse, we used negative conductance coupling between the neurons. Although the synaptic current remained a linear function of the membrane potential difference, negative conductance coupling was in some aspects similar to a mutual inhibitory chemical connection but without delay, threshold or non-linear properties. The effect observed upon coupling in the chaotic EN to the PD was even more dramatic (Fig. 2F), although the neurons were bursting in anti-phase. A clearly periodic bursting pattern appeared after initiating this coupling, and the time series of the PD was virtually indistinguishable from that seen in the intact CPG. Inhibitory postsynaptic potentials from EN were apparent in the membrane potential of PD, and strong rebound plateaus followed the hyperpolarized states. These data clearly demonstrate that regular and robust oscillatory patterns characteristic of the intact pyloric CPG can be achieved by simply coupling the intrinsically irregular/chaotic EN to the PD neuron. As a control, we performed experiments with constant negative current injection into the PD neuron and with unidirectional coupling between EN and PD. In that case, we did not observe regularization of PD. Regularization appears only when the PD is connected bidirectionally to the EN.

Analysis of spike time data: Spike density functions clearly showed the most prominent features of the EN–PD interaction and revealed new details about this process. The SDFs of the uncoupled neurons, when both were firing in an irregular pattern, were aperiodic and random-like (not shown). The corresponding phase-portrait possesses

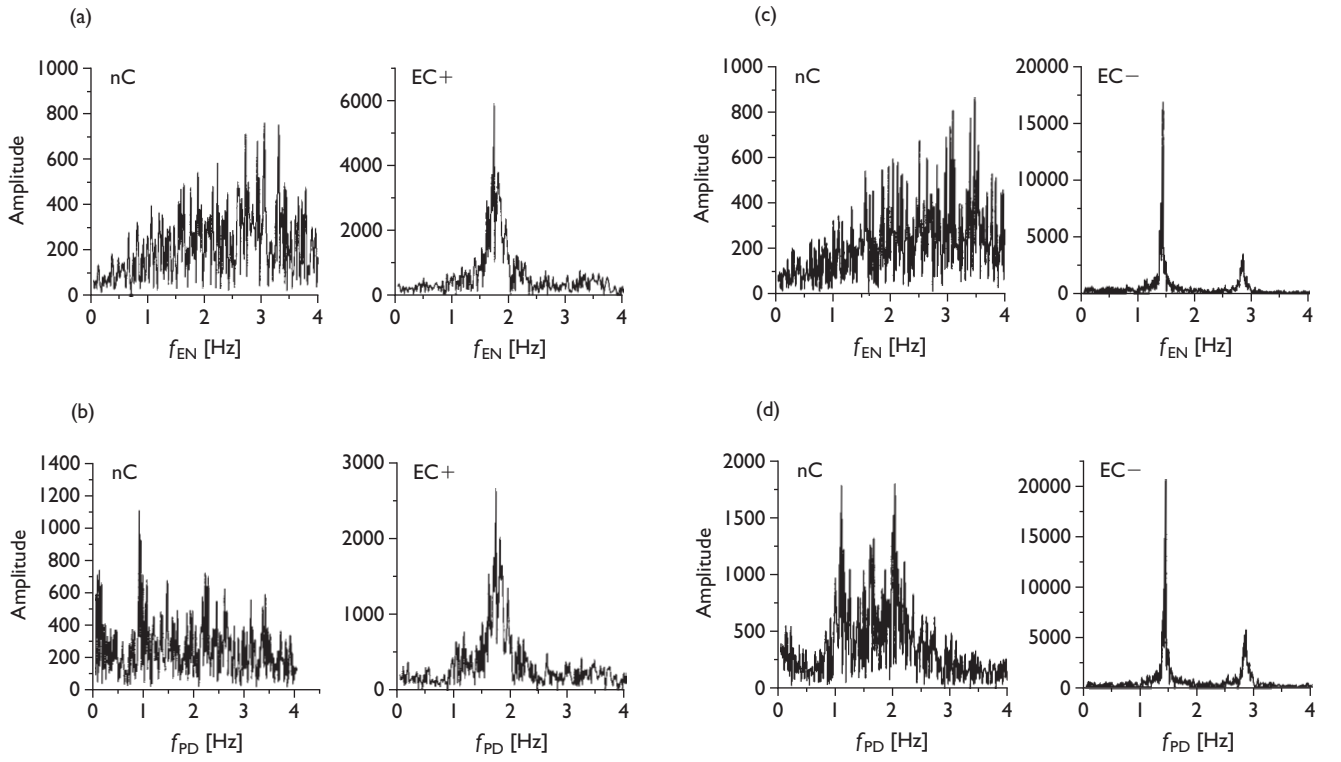

Fig. 4. Fourier transforms of the spike density functions of free-running and coupled EN and PD neurons. The spectra were calculated from simultaneous sections of the SDFs. (**a**,**c**) EN; (**b**,**d**) PD. Broad band, 'noisy' Fourier spectra imply irregular dynamics of both the EN and the PD when disconnected (nC). A very weak periodicity with 1 Hz frequency can be detected in the free-running PD. Clear peaks appear as a consequence of periodic bursting behavior when using a positive (EC+) or negative (EC−) conductance synapse.

no apparent structure or orientation (Fig. 3C, left). Positive electrotonic coupling led to synchronized oscillations in the SDF (Fig. 3A) and diagonal trajectories in the phase-portrait (Fig. 3C, right). SDFs in negative conductance coupling experiments exhibited a similar behavior. SDFs of both EN and PD are precisely periodic (Fig. 3B), and the phase-portrait consists of a tight trajectory with negative slope (Fig. 3D, right). The Fourier transforms of the SDFs of uncoupled irregular EN and PD neurons had a broad band 'noisy' distribution characteristic of chaotic dynamics (Fig. 4). Sharp peaks in the Fourier spectra appear as a consequence of periodic bursting when the neurons were connected. The frequency of the oscillation (1.8 and 1.4 Hz with positive and negative coupling, respectively) was close to the pyloric rhythm observed in the intact preparation.

Dependence of the effects on coupling strength: The experiments involved systematic scanning of the parameters of the EN, tuning the shape of the oscillation, as well as changing the synaptic strength between the electronic and pyloric neuron. ISI sequences measured from a long-term experiment and return maps of the same data are shown in Fig. 5. The intrinsically chaotic EN was coupled to an irregular PD neuron via positive conductance electrotonic synapse. The 'burstiness' of the firing patterns depended on the strength of the connection. Weak coupling resulted in minor changes in the PD, whereas strong coupling resulted in clear burst activity, with a bimodal ISI distribution. The triangular structure of the ISI return map shown in Fig. 5C and D is characteristic of periodically bursting neurons. This pattern emerged after electrically coupling an intrinsically chaotic EN to the isolated PD. Negative conductance coupling had a stronger regularizing effect on the firing of the neurons in all cases. The magnitude of the changes in the ISI pattern of the EN was a function of the connection strength as well as the firing pattern set prior to the coupling. Switching off the electrotonic connection commonly led to quick restoration of the irregular firing or bursting pattern in PD.

DISCUSSION

Several implementations of neural models in electronic circuits have been used to capture aspects of neuronal function and organization in what recently has been called neuromorphic systems [17,18]. Mixed circuits consisting of biological neurons and electronic devices are particularly useful in studying small neural systems such as those of CPGs. Only in very few instances have analog implementations of model neurons and synapses actually been used to interact with biological cells. An analog network of coupled subthreshold oscillators was connected to olivary neurons in Yarom's work [19] and the mechanisms of synchronized neural oscillations were investigated. In another study Le Masson and coauthors used BiCMOS implementations of complex, multiparameter Hodgkin–Huxley models [20]. Several features of the neural function of stomatogastric neurons as well as thalamocortical cells

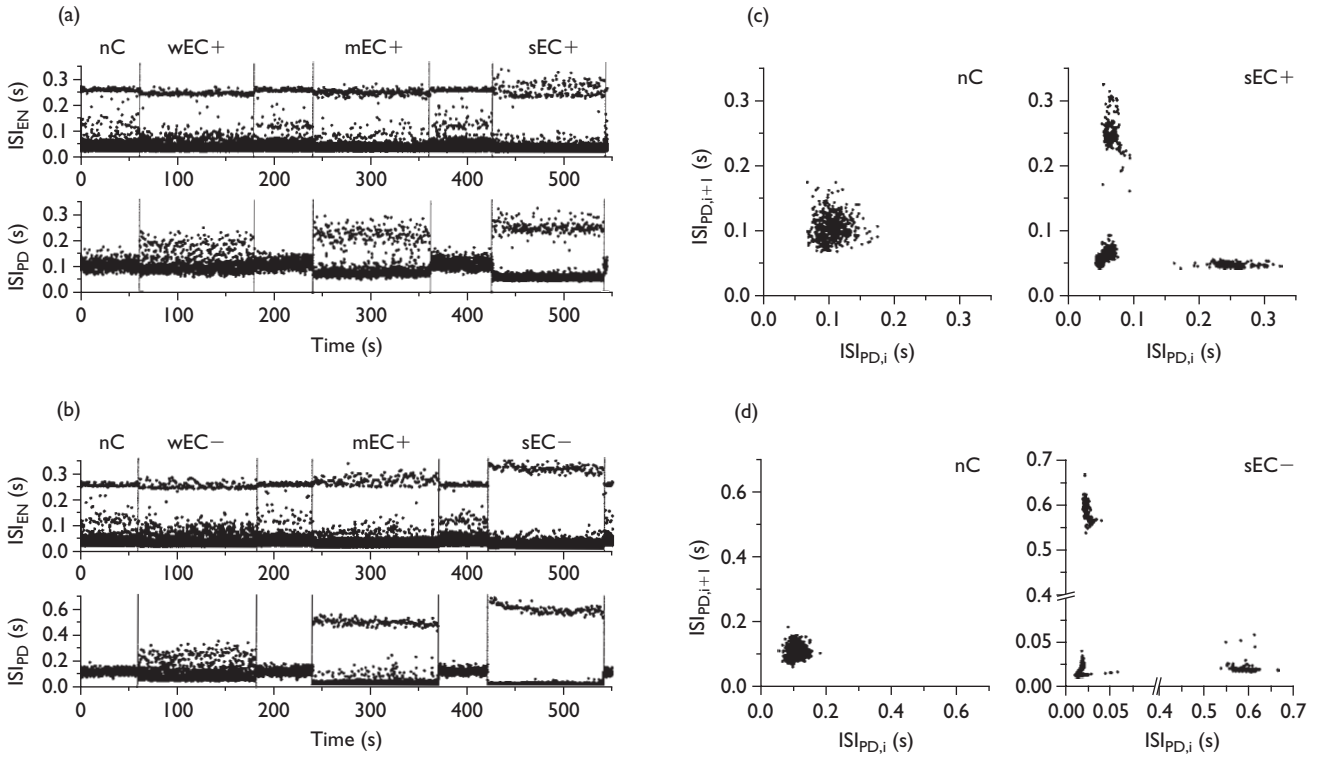

Fig. 5. Interspike-interval sequences and return maps. (**a**,**b**) Time *vs* ISI graphs calculated from 550 s long spike trains. Vertical lines mark the onset and release of the electrical connection with various strength (wEC+/−: weak, mEC+/−: moderate and sEC+/−: strong). (**c**,**d**) ISI return maps constructed from various parts of the corresponding ISI sequences of the PD neuron. A diffuse cloud of points indicates highly irregular spiking in the isolated PD. The triangular form appears as a consequence of burst generation when using strong coupling (sEC+ and sEC−).

were reconstructed by these electronic models. A similar approach has been utilized by constructing artificial synaptic connections between existing biological neurons using advanced computer techniques [21,22]. Clearly, response-dependent stimulation of biological neurons have proven a fruitful method to study details of cellular excitability or network dynamics.

In our work we used a simplified, yet realistic, electronic model of a stomatogastric neuron. Instead of making an effort to simulate all ionic conductances contributing to the membrane potential of the living lobster neurons, we built a three-variable analog circuit. Previously we have shown that computational models of Hindmarsh–Rose type neurons reproduce several aspects of the neural function of spiking/bursting neurons [12]. These mathematical models exhibited various firing/bursting patterns and bifurcations similar to those seen in living stomatogastric neurons, when coupled in dynamic clamp experiments [22].

In this note we have presented evidence that two different irregular neurons, one biological and one electronic, are able to produce regular rhythm, when coupled electrically over a wide range of coupling strengths. Regular rhythms can be produced by intrinsically nonregular neurons. These results also suggest that it is not necessary to reproduce all of the biological aspects of the operation of nerve cells to address issues of communication and cooperation among oscillating neurons in CPG-like networks. The full mechanism of the observed regularization phenomenon is not clearly understood yet and requires additional investigation. However, from the dynamical systems theory point of view such behavior is plausible: coupling two different chaotic elements in fact means the creation of a new dynamical system with new types of possible behavior. In our case the slow bursting dynamics suppresses the chaotic instability of spikes and leads to regular synchronized oscillations.

CONCLUSION

We have shown here the broad value of a 'mixed technology' in the investigation of important physiological problems related to the dynamics of small neural networks. The interaction of an EN with groups of living neurons provides the potential for changing the connectivity and topology of neural networks. It also allows better understanding of the roles of intrinsic and synaptic properties of neurons in rhythm generation or information processing. The noteworthy simplicity of our EN suggests that these circuits may be used as replacement neurons in other CPGs that appear as control systems in more complex organisms. The application of these mixed systems to robotics may also be possible.

REFERENCES

1. Marder E. *Neuroscientist* **3**, 295–302 (1997).
2. Bal T, Nagy F and Moulins M. *J Comp Physiol* **163**, 715–727 (1988).
3. Elson RC, Huerta R, Abarbanel HDI *et al. J Neurophysiol* **82**, 115–122 (1999).

4. Rabinovich MI and Abarbanel HDI. *Neuroscience* **87**, 5–14 (1998).
5. Hayashi H and Ishizuka S. *J Theor Biol* **156**, 269–291 (1992).
6. Mpitsos GJ, Burton RM, Creech HC and Soinila SO. *Brain Res Bull* **21**, 529–538 (1988).
7. Marder E and Calabrese RL. *Physiol Rev* **76**, 687–717 (1996).
8. Harris-Warrick RM, Marder E, Selverston AI and Moulins M. *Dynamic Biological Networks, The Stomatogastric Nervous System*. Cambridge MA, MIT Press, 1992.
9. Mulloney B and Selverston AI. *J Comp Physiol* **91**, 1–32 (1974).
10. Selverston AI and Miller JP. *J Neurophysiol* **44**, 1102–1121 (1980).
11. Hindmarsh JL, and Rose RM. *Proc Roy Soc Lond B* **221**, 87–102 (1984).
12. Rabinovich MI, Abarbanel HDI, Huerta R *et al. IEEE Trans Circ Systems* **44**, 997–1005 (1997).
13. Szűcs A. *J Neurosci Methods* **81**, 159–167 (1998).
14. Paulin MG. *Biol Cybern* **66**, 525–531 (1992).
15. Johnson BR, Peck JH, and Harris-Warrick RM. *J Comp Physiol* **172**, 715–732 (1993).
16. Abarbanel HDI. *Analysis of Observed Chaotic Data*. New York: Springer-Verlag, 1996.
17. Douglas R, Mahowald M and Mead C. *Ann Rev Neurosci* **18**, 255–281 (1995).
18. Mead C. *Analog VLSI and Neural Systems.* Reading, MA: Addison-Wesley, 1989.
19. Yarom Y. *Neuroscience* **44**, 263–275 (1991).
20. Le Masson S, Laflaquiére A, Bal T and Le Masson G. *IEEE Trans Biomed Eng* **46**, 638–645 (1999).
21. Sharp AA, O'Neil MB, Abbott LF and Marder E. *Trends Neurosci* **16**, 389–394 (1993).
22. Elson RC, Selverston AI, Huerta R *et al. Phys Rev Lett* **81**, 5692–5695 (1998).

Review TRENDS in Neurosciences Vol.27 No.4 April 2004

The dynamic clamp comes of age

Astrid A. Prinz, L.F. Abbott and Eve Marder

Volen Center and Department of Biology, Brandeis University, Waltham, MA 02454-9110, USA

The dynamic clamp uses computer simulation to introduce artificial membrane or synaptic conductances into biological neurons and to create hybrid circuits of real and model neurons. In the ten years since it was first developed, the dynamic clamp has become a widely used tool for the study of neural systems at the cellular and circuit levels. This review describes recent state-of-the-art implementations of the dynamic clamp and summarizes insights gained through its use, ranging from the role of voltage-dependent conductances in shaping neuronal activity to the effects of synaptic dynamics on network behavior and the impact of *in vivo*-like input on neuronal information processing.

The term dynamic clamp refers to a variety of hardware and software implementations used to create artificial conductances in neurons. Since its introduction more than ten years ago [1–3], the dynamic clamp has become a standard tool of electrophysiology, used in a wide variety of experimental preparations to address a host of different issues. This review describes how the dynamic clamp creates an artificial conductance, provides an overview of some of the different dynamic-clamp systems currently in use and discusses what can and has been achieved using the technique.

What is the dynamic clamp?

In contrast to conventional voltage- or current-clamp recording configurations, the dynamic clamp effectively alters the conductance of a neuron [1,2]. It does so by using the measured membrane potential to control the amount of current injected into a neuron. To simulate a particular conductance, the dynamic clamp computes the difference between the measured membrane potential and the reversal potential for that conductance, multiplies this 'driving force' by the desired amount of conductance, and injects the resulting current into the neuron. Accurate dynamic-clamp performance requires uninterrupted, rapid sampling of the membrane potential and fast computation of the current to be injected. If the sampling and computation are fast enough, the electrophysiological effects of any set of ion-conducting channels can be reproduced as if these were located at the site of voltage measurement and current injection.

Any time- or voltage-dependent conductance that has been described mathematically and can be simulated on a computer can be introduced into a neuron using the dynamic clamp. For a voltage-dependent conductance, the injected current is determined by a set of differential equations that describe the voltage and time dependence of the conductance. For a synaptic conductance, the current injected by the dynamic clamp is computed on the basis of presynaptic input that is either recorded from another neuron, or generated by a model neuron or by a descriptive model of typical *in vivo* input.

Dynamic-clamp implementations

Obtaining sufficiently high update rates in the first dynamic-clamp implementations of the early 1990s pushed the limits of computer and data acquisition board technologies available at that time. As a result, some of the earliest dynamic-clamp programs were written in machine language [1,2] and used look-up tables [3], and some implementations used digital signal processing (DSP) boards to achieve the required speed [4]. Today, computers and boards are so fast that hardware speed is no longer a significant issue, and many different dynamic-clamp systems have been developed and used in several laboratories around the world. These systems vary considerably in their front-end user interfaces, in how readily programmable they are, in how many different conductances can be simulated, in how many neurons can be studied simultaneously, in whether they display and save voltage and current traces online, and in their cost. Our conservative estimate is that there are at least 20 different dynamic-clamp setups in use in laboratories around the world today, and many more papers than can be cited here have been published with some version of dynamic-clamp implementation. Table 1 lists several of the dynamic-clamp systems presently in use to illustrate the diversity of approaches, hardware, and features. Because computers and boards change so quickly, this list provides only a snapshot of the present situation.

Currently available implementations of the dynamic clamp include applications that run under the Windows or Real-Time Linux operating systems, systems that use embedded processors or DSP boards, and versions that use analog devices. The advantages and disadvantages of these different approaches are outlined briefly below.

Windows-based applications

Windows-based dynamic-clamp systems typically achieve update rates of 2–20 kHz, depending on the computational load for the particular conductances being simulated [5–7]. This is fast enough for most purposes, but extremely fast conductances, such as those of fast Na^+ currents, can only be approximated crudely. An additional problem stems from the fact that

Corresponding author: Astrid A. Prinz (prinz@brandeis.edu).

 0166-2236/$ - see front matter doi:10.1016/j.tins.2004.02.004

Table 1. Recent examples of dynamic-clamp implementations[a]

	Windows-based	Real-time Linux-based		Embedded processor or DSP	Analog device	
References	[6]	[9]	[10]	[12]	[14]	Instrutech, ITC-18
URL	inls.ucsd.edu/~rpinto/	www.bu.edu/ndl/rtldc.html	www.neuro.gatech.edu/mrci/	NA	NA	www.instrutech.com
Programming language	C++	C, C++for user interface	MRCI modeling language, C	Real-Time LabView	NA	NA
Update rate[b]	10 kHz	20 kHz[d]	30 kHz	40 kHz	NA	50 kHz
Existing applications	Artificial conductances; artificial chemical or electrical synapses between up to four cells	Artificial conductances; hybrid two-cell networks; adding multiple compartments	Artificial synaptic inputs; hybrid two-cell networks	Artificial conductances; artificial chemical synapses; recording current–voltage curves	Artificial synaptic inputs	Artificial synaptic inputs
Number of channels[c]	Four in, four out	Two in, two out[d]	Two in, two out	Two in, one out	Four in, four out	Four in, four out
User interface	Graphical	Graphical	Command line	Graphical	NA	NA
Saves traces?	No	Yes	Yes	Yes	NA	NA
Displays traces?	No	Yes	No	Yes	NA	NA

[a]Abbreviations: DSP, digital signal processing; MRCI, model reference current injection; NA, not available.
[b]Update rates vary depending on the computational load. Updates rates given here are maximum values of published versions of the systems and will increase with time.
[c]Channel numbers given here are those of published versions of the systems. Most systems can be modified to handle larger channel numbers if different hardware is used.
[d]Newer, unpublished versions of this system can achieve update rates of up to 40 kHz, and can handle as many as 16 input and 2 output channels (J. White, pers. commun.).

any Windows-based program must deal with operating system interrupts through which Windows distributes processor time between different tasks. These can lead to discontinuities and gaps in dynamic-clamp operation and prevent real-time performance, even at low update rates.

The Windows-based dynamic clamp described by Pinto and colleagues [6] uses a Digidata 1200 board (Axon Instruments, http://www.axon.com) for data acquisition and digital-to-analog conversion. Because such boards are commonly used (and this dynamic-clamp software is available for free download from the developers), this particular implementation requires no more of a financial investment than that required for a standard electrophysiology rig.

Real-Time Linux-based applications

Recently developed versions of the dynamic clamp that operate under Real-Time Linux avoid the interrupt problem of a Windows-based system and can achieve update rates of 20–50 kHz, depending on the data acquisition board [8–10]. At the moment, the installation and operation of the real-time operating system requires considerable expertise, which can deter some users. However, with several laboratories developing more user-friendly Real-Time Linux-based dynamic-clamp systems, the installation and use of these systems is rapidly becoming easier.

Embedded-processor and DSP-based systems

Update rates of 20–50 kHz can also be achieved by using an embedded processor or DSP board [4,11–13]. These devices can be controlled by a host computer and programmed through a graphical programming language with a user-friendly interface [12] or through Real-Time Workshop (The MathWorks, http://www.mathworks.com), but these advantages literally come at a high price. The costs for the additional hardware, necessary drivers, and compiler software can be between US$5000 and US$10 000.

Analog devices

For some applications, the dynamic clamp can be implemented using analog circuits that perform the basic subtraction and multiplication operations needed to convert a desired conductance and a measured potential into an injected current [14]. These analog circuits are commercially available (e.g. SM-1 from Cambridge Conductance, http://homepage.ntlworld.com/cambridge.conductance; or ITC-18 from Instrutech Corporation, http://www.instrutech.com). The advantage of an analog approach is its high speed, which is essentially instantaneous on the scale of typical membrane and synaptic time constants. However, the basic analog system only makes the conversion from conductance to injected current. For any application other than the simulation of a constant conductance, these systems must be driven by a digital computer programmed to calculate the desired conductance and drive the analog circuitry. As a result, analog systems are most useful in cases where synaptic, rather than voltage-dependent, conductances are being simulated.

Applications of the dynamic clamp

Uses of the dynamic clamp have been divided here into five broad categories: simulation of voltage-independent conductances, simulation of voltage-dependent conductances, simulation of synapses between neurons, construction of biological–computer hybrid circuits, and simulation of *in vivo* synaptic input. For each of these categories, a single example from the many possibilities in the literature has been chosen to illustrate what can be achieved and what has been learned using these approaches. Additional selected studies using the same dynamic-clamp approach are briefly summarized for each category.

Effects of voltage-independent conductances

Simulating a voltage-independent conductance is the simplest thing that can be achieved with the dynamic clamp (Figure 1a) but, nevertheless, it is useful for studying the effects of leakage conductances or ligand-gated conductances on neuronal dynamics. Figure 1b provides an example in which a dynamic clamp was used to duplicate the effect of a ligand-gated conductance with a reversal potential of −75 mV in a neuron of the crustacean stomatogastric ganglion to study the effects of a voltage-independent GABA conductance [2].

Dynamic-clamp conductances act in parallel with the normal membrane conductances of the neuron, and the interaction between the added and existing conductances is what makes such manipulations interesting. In the example shown in Figure 1b, current pulses of constant amplitude were introduced to show that the dynamic clamp was modifying the conductance of the neuron (Figure 1b, bottom) in exactly the same way as a bath application of GABA (Figure 1b, top). The dynamic clamp mimics both the GABA-induced hyperpolarization and the reduction in the voltage response to constant-amplitude current pulses caused by the GABA conductance. In a related approach, the dynamic clamp has been used to add artificial GABA conductances in thalamocortical relay cells to elucidate the role of GABA-mediated inhibitory postsynaptic potentials (IPSPs) in rebound burst firing and burst inhibition [15,16].

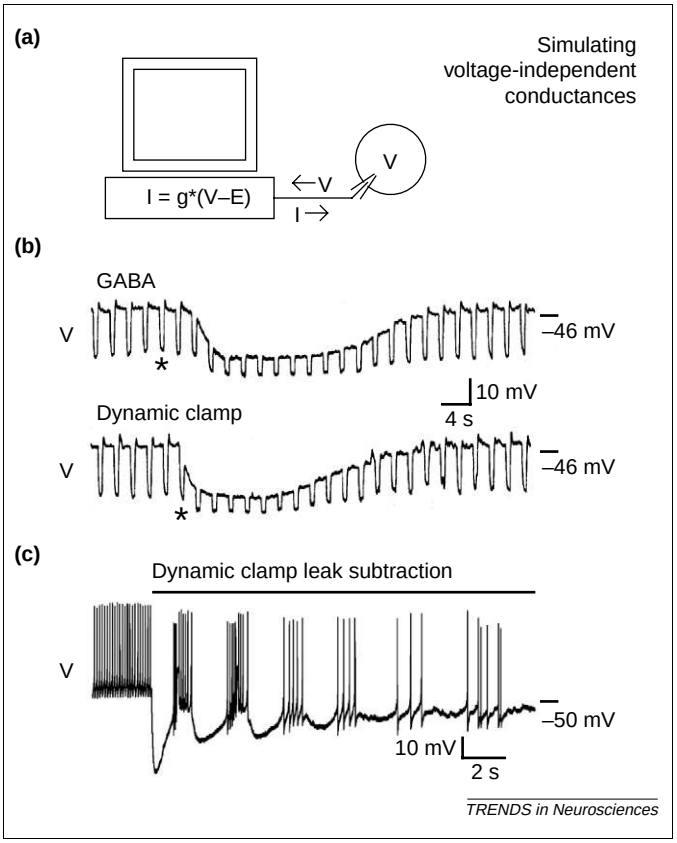

Figure 1. Using the dynamic clamp to simulate voltage-independent conductances. **(a)** Schematic of the experimental configuration. The dynamic clamp computes the current, I, flowing through a voltage-independent conductance, g, as g multiplied by the instantaneous driving force, V–E, where E is the reversal potential and V is the membrane potential. In every cycle of dynamic-clamp operation, V is measured and fed into the computer, I is computed based on the momentary value of V, and I is injected into the cell. Voltage measurement and current injection can be made through the same electrode with discontinuous clamp techniques, or through two separate electrodes. **(b)** Voltage traces recorded from a cultured crab stomatogastric neuron during 30 s bath application of 0.1 mM GABA (top) and during dynamic-clamp injection of an exponentially rising ($t = 5$ s) and falling ($t = 15$ s) GABA conductance with a reversal potential of -75 mV (bottom). The starts of bath and dynamic-clamp application are indicated by asterisks. During both runs, current pulses of -0.5 nA were applied every 3 s to illustrate the change in input conductance. Adapted, with permission, from Ref. [2]. **(c)** Voltage trace from a leech heart interneuron before and during injection of a negative leak conductance of -6 nS with a reversal potential at 0 mV. The leak subtraction compensates for the effect of sharp microelectrode penetration, which suppresses bursting. Adapted, with permission, from Ref. [17] © (2002) by the Society for Neuroscience.

In addition to being added, conductances can, with some restrictions, be subtracted using the dynamic clamp. Figure 1c shows an example. The leakage conductance introduced by the electrode penetration required for intracellular recordings made with sharp electrodes is a potential source of distortion of the natural activity of the recorded neuron. Figure 1c shows an example in which the dynamic clamp was used to simulate a negative conductance designed to cancel out the impact of the leakage introduced by electrode penetration [17]. Addition of an artificial leak conductance had been shown previously to switch leech heartbeat interneurons from an active state with high-frequency bursting to an inactive state [18]. Because of this sensitivity of bursting to additional leak conductance, the electrode leak was removed by the dynamic clamp. The bursting activity that is the natural mode of operation for this neuron was revealed only after the leakage conductance introduced by electrode penetration was subtracted using the dynamic clamp.

Taken together, dynamic-clamp studies that simulate voltage-independent conductances in different preparations demonstrate important roles for seemingly simple leak and ligand-gated currents in shaping neural activity. The importance of voltage-independent conductances is further supported by reports that dynamic-clamp simulated leak current can increase motoneuron spiking in the mammalian spinal cord [19] and that adding a Ca^{2+} window current or subtracting leak current can render thalamocortical neurons bistable [20].

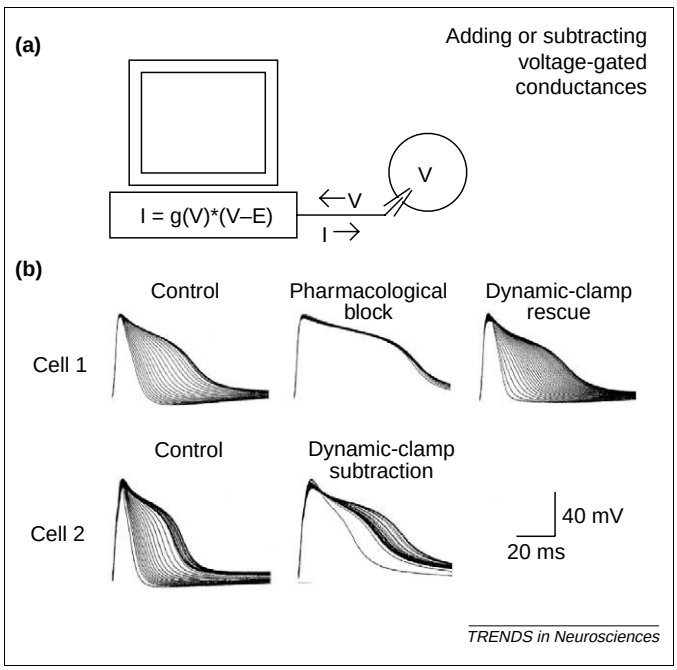

Figure 2. Adding or subtracting voltage-dependent conductances. **(a)** Schematic of the experimental configuration. The dynamic-clamp current is computed as in Figure 1, but in this case the conductance, g, varies with time and depends on the membrane potential, V. **(b)** Each panel shows 65 superimposed spikes from an *Aplysia* R20 neuron in response to 7 Hz current pulse injection. In control conditions, the action potential is initially narrow and broadens during the spike train (top-left). Spike broadening is abolished in 50 mM tetraethylammonium (TEA) and 10 mM 4-aminopyridine (4-AP; top-middle) and rescued when an A-type and a delayed-rectifier K^+ current are added with the dynamic clamp (top-right). In a different cell (bottom), the action of the blockers was approximated by subtracting these two conductances with the dynamic clamp. Adapted, with permission, from Ref. [21] © (1996) by the Society for Neuroscience.

Effects of voltage-dependent conductances

The dynamic clamp can be used to introduce voltage-dependent conductances into a neuron (Figure 2a), which is useful for exploring the impact of different intrinsic membrane conductances on neuronal activity. Specific conductances already present in the ensemble of intrinsic conductances in the neuron can be augmented or decremented to reveal the role that they play in generating its particular pattern of firing. Used in this manner, the dynamic clamp supplements more traditional methods of blocking conductances pharmacologically because it allows for very specific targeting and very precise control of the amount of the modification being made on any conductance. In addition, non-native voltage-dependent conductances can be added to the natural complement of the neuron to see what novel dynamics can be generated.

Figure 2b provides an example of this type of manipulation [21]. Each panel shows 65 superimposed spikes recorded from an *Aplysia* R20 neuron responding to the injection of current pulses at 7 Hz. In control conditions, the action potential broadens during repetitive spiking (Figure 2b, top-left). This broadening was abolished when A-type and delayed-rectifier K^+ conductances were pharmacologically blocked because the initial spikes were already broad (Figure 2b, top-middle). Spike broadening was restored under the pharmacological block by adding these conductances back using the dynamic clamp (Figure 2b, top-right). This result clearly implicates A-type and delayed-rectifier K^+ conductances in the phenomenon of spike broadening. The dynamic clamp could also partially duplicate the effect of the pharmacological blockade when it was used to subtract these two conductances (Figure 2b, bottom).

Dynamic-clamp simulation of voltage-dependent conductances has been used in stomatogastric ganglion neurons to investigate the roles of transient K^+ currents and hyperpolarization-activated inward currents [22,23], to study the effects of a neuromodulatory peptide-elicited current on the output of a rhythmic network [24], to show that a slow K^+ conductance can underlie cellular short-term memory [25], and to demonstrate how the relative amounts of different Ca^{2+} and K^+ conductances can determine whether a neuron is silent, spikes tonically, or bursts [26]. Artificial voltage-dependent currents have been used in preparations as diverse as pancreatic β-cells [27,28], thalamocortical [29] and neocortical neurons [5], and hippocampal interneurons [11]. The dynamic-clamp studies in these systems have identified individual voltage-dependent conductances involved in subthreshold membrane resonances [5], high-frequency spiking [11], bursting [27–29] and delta oscillations [29], and have thus contributed considerably to our understanding of dynamic processes in these systems.

Building and modifying neuronal circuits with artificial synapses

Thus far, we have focused on applications in which the dynamic clamp is used to introduce or remove membrane conductances to assess their role at the single neuron level. The remaining examples show uses of the dynamic clamp for creating artificial synaptic conductances. In these applications, the neuron being dynamically clamped acts as the postsynaptic element, and another neuron or a computer model acts as the source of presynaptic input. Here, cases in which the presynaptic element is another neuron are considered. As illustrated in Figure 3a, this approach requires recording the membrane potential of the 'presynaptic' neuron and using it and the dynamic clamp to control current injection into the 'postsynaptic' neuron. A synapse in an existing circuit can be augmented or decremented to study its effect on network activity, or a simulated synapse can be introduced where none existed before, allowing for the construction and study of completely novel neural circuits. The dynamic clamp provides the experimenter with complete control over the strength and other properties of these artificial synapses.

Figure 3b shows an example in which a so-called 'half-center' oscillator was constructed by connecting two stomatogastric ganglion neurons with reciprocally inhibitory synapses that were simulated with the dynamic clamp [6]. To construct the half-center oscillator, the two neurons were first isolated and then connected by artificial

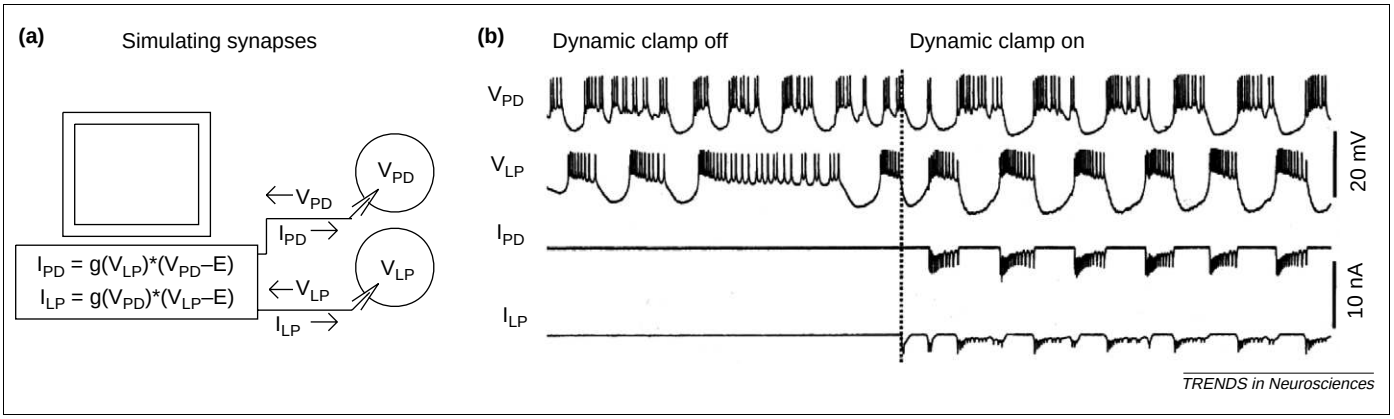

Figure 3. Creating artificial synapses between real neurons. **(a)** Schematic of the experimental configuration. The current that is injected into the postsynaptic neuron (I_{PD} or I_{LP}) is the product of the synaptic conductance, which depends on the membrane potential of the presynaptic neuron, and the driving force. **(b)** Voltage and dynamic-clamp current traces for a pyloric dilator (PD) and a lateral pyloric (LP) neuron of the lobster stomatogastric ganglion before and after the dynamic clamp was switched on. The artificial synapses induced the neurons to oscillate in antiphase. Adapted, with permission, from Ref. [6].

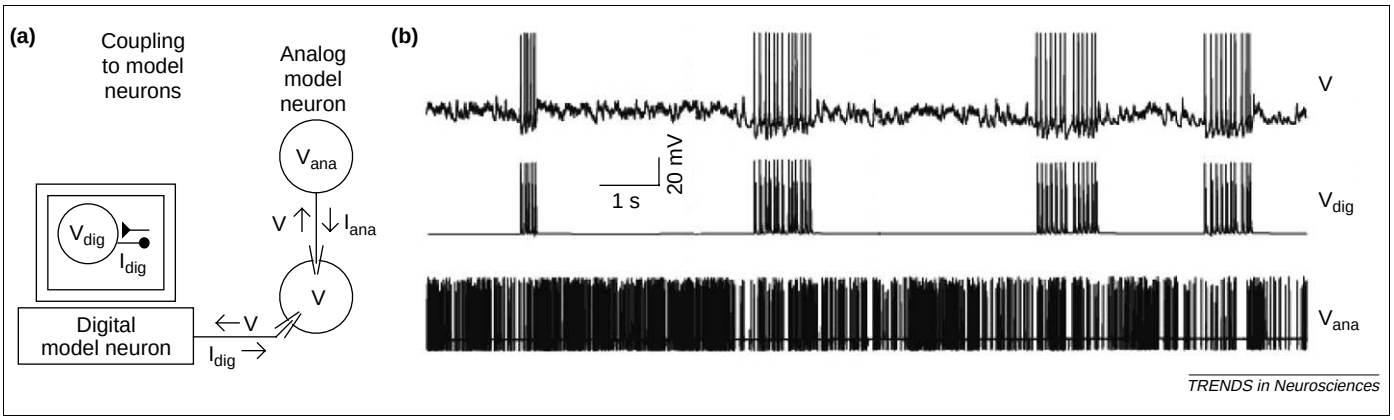

Figure 4. Building hybrid circuits of real and model neurons. **(a)** Schematic of the experimental configuration. The computer integrates the differential equations that describe the digital model neuron (dig) and its synaptic connections, while the analog model (ana) is an electrical circuit that mimics another neuron and its synapses. **(b)** Voltage traces from a thalamocortical cell (V), an analog retinal model neuron (V_{ana}) and a digital model reticular interneuron (V_{dig}). The thalamocortical neuron receives excitation from the analog and inhibition from the digital model neuron and excites the digital model neuron. The hybrid circuit generates spontaneous spindle activity similar to that in the sleep-like state. Adapted, with permission, from Ref. [13].

synapses. The anti-phasic oscillations exhibited by the two cells with artificial synapses are reminiscent of their behavior in the intact circuit, where they mutually inhibit each other through biological synapses. In an earlier study connecting two other stomatogastric ganglion neurons with reciprocal inhibitory connections, artificial synaptic connections allowed the examination of how the presence, frequency, and phase relations of oscillations depended on synaptic parameters and on intrinsic membrane conductances [30].

The approach of coupling two or more biological neurons with artificial inhibitory [6,30–33] or electrical [34–37] synapses has been used to study the effects of synapse strength [38] and dynamics on neuronal firing patterns [36], on the synchronization between oscillatory neurons [30,33,36,37] and rhythmic circuits [32], and on the intraburst firing pattern of bursting neurons [31].

Building hybrid computer–biological neural circuits

The dynamic clamp can provide an approach to the study of neural systems that falls midway between computer modeling and experimental electrophysiology. In modeling studies, we often want to assess the role of certain elements, such as individual conductances or synapses, that we might be able to model accurately. However, in a conventional modeling approach, we must incorporate these well-described elements into a model of a neuron or neural circuit that is inevitably much cruder. The dynamic clamp allows us to manipulate the well-modeled elements we wish to study with the same degree of precision and freedom that we have in a model, while allowing them to interact with real neurons or neural circuits, with all their complexities intact. Used properly, the dynamic clamp allows studies that combine the best features of computer modeling and experimental electrophysiology. An excellent example is the construction of hybrid circuits that involve interacting computer-modeled and biological elements (Figure 4a).

Figure 4b shows an example in which a real thalamocortical neuron was coupled using the dynamic clamp to two model neurons, one simulated by a digital computer and the other by an analog circuit [13]. The digital model neuron represented a reticular interneuron, while the analog circuit modeled a retinal ganglion cell. When coupled together, these three elements formed a circuit that could generate the type of spindle activity seen in the thalamus during sleep states. During sleep, the correlation between spikes in retinal ganglion cells and spikes in thalamocortical neurons is low, so that the cortex is functionally disconnected from its sensory drive. Systematic variation of the artificial inhibitory synapse from the model reticular interneuron to the biological thalamocortical neuron showed that the strength of this connection regulates the temporal correlation between the sensory input and the thalamocortical cell firing pattern [13].

Similar hybrid network configurations have been used to determine the effect of synaptic depression on oscillation frequency and bistability in reciprocally inhibitory pairs of neurons [7,39], to probe aspects of pain processing in the spinal cord [40], and to examine the effect of electrical coupling strength on synchronization of rabbit sinoatrial node cells [41].

Simulating in vivo *conditions*

Neurons and neural circuits are frequently studied in slice preparations. Slice preparations have distinct advantages in terms of accessibility for visualization and recording, but the disadvantage of being relatively silent. Because each neuron receives much less ongoing synaptic input in the slice than it would in an intact brain, neurons in slices are studied in an environment that is significantly different from that in which they normally operate. The dynamic clamp offers a way of studying neurons in slices while simulating *in vivo* synaptic input.

Figure 5a shows a dynamic clamp setup used to simulate *in vivo*-like synaptic input, both excitatory and inhibitory, entering a cortical pyramidal neuron [14]. In the absence of this input, the neuron fired regularly in response to current injection (Figure 5b, top), but when the simulated synaptic bombardment was introduced, the response was irregular with large subthreshold voltage fluctuations, as seen *in vivo* (Figure 5b, bottom). Figure 5c

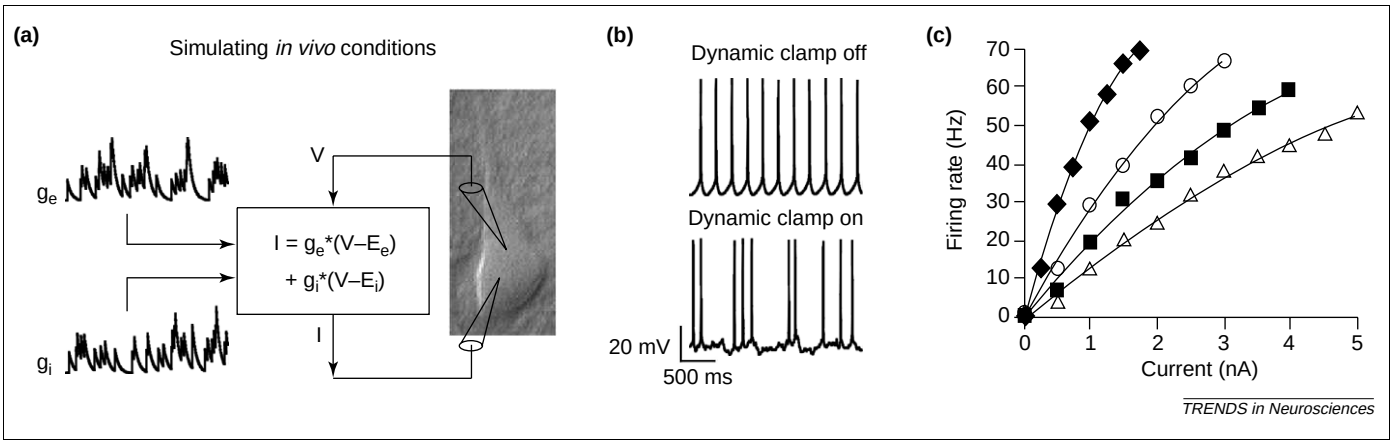

Figure 5. Simulating *in vivo* conditions in a slice preparation. **(a)** Schematic of the experimental configuration used to simulate balanced excitatory and inhibitory synaptic background conductances in a pyramidal neuron from a slice of rat somatosensory cortex. The dynamic clamp computes the total synaptic current produced by a stochastic model of ongoing cortical activity. The total synaptic current is the product of *in vivo*-like conductances g_e and g_i and the appropriate driving forces for excitatory (e) and inhibitory (i) synapses. **(b)** Voltage traces from a pyramidal neuron in response to constant driving current without (top) and with (bottom) artificial background synaptic input. **(c)** Firing rates of a neuron as a function of constant driving current without simulated background synaptic input (diamonds), with a given amount of background synaptic input (circles), with twice that amount (squares) and with three times that amount (triangles). Changing the level of synaptic background input modulates the gain of the neuron. Reproduced, with permission, from Ref. [14].

indicates that modulation of this synaptic bombardment can have important functional consequences. The slopes of the firing-rate versus input current curves shown in this figure decrease for increasing amounts of total dynamic-clamp simulated background synaptic input. This suggests that background synaptic input *in vivo* can act as a gain control mechanism [14,42,43]. The results of Figure 5c depend on the conductance modification that is due to the simulated synaptic input, so they could not have been obtained on the basis of current injection without using the dynamic clamp.

The dynamic clamp has been used to mimic realistic synaptic input patterns in many different neural systems, including auditory brainstem [44], lateral geniculate nucleus [45], basal ganglia [46], cerebellum [43,47–49], cortex [14,50,51], and avian nucleus laminaris [52]. In these systems, the technique has provided insights about the role of timing [47,48], rate [46], and synchrony [50,52] of synaptic inputs in postsynaptic signal processing.

Limitations of the dynamic clamp

A major limitation of the dynamic clamp is that the conductances it simulates are restricted to the site of current injection. As a result, conductances located far from the injection site can be mimicked only approximately. Normally, the injection site is the soma, but the advent of dendritic patch recording makes it feasible to simulate and apply conductances to dendrites. It would be particularly interesting to compare the effects of dynamic-clamp simulations carried out using dendritic and somatic injection sites. An alternative approach, which is useful for simulating dendritic conductances with somatic current injection, is to modify the current being injected by the dynamic clamp to include dendritic cable effects on the basis of a multi-compartment model.

Another limitation is that the dynamic clamp duplicates the electrical but not the signal conduction consequences elicited by specific ionic currents. In particular, with conventional electrode solutions, the dynamic clamp can simulate the electrical current from a set of Ca^{2+} channels, but it does not reproduce the changes in intracellular Ca^{2+} concentration that normally accompany the gating of such channels. In some cases, this limitation can be exploited to isolate voltage-mediated effects from other mechanisms.

Finally, the dynamic clamp shares a limitation with traditional current- and voltage-clamp techniques: artifacts of electrode resistance and capacitance. These artifacts can be minimized by using low-resistance electrodes, by using separate electrodes for voltage recording and current injection, or by temporally separating recording and injection through a single electrode using the discontinuous current-clamp technique.

Concluding remarks

To understand how neurons and neural circuits work, we must do more than simply watch them in action. We must probe and perturb them in various ways and study how they respond. Current clamping is one method for probing neuronal dynamics, and voltage clamping to realistic waveforms can provide interesting insights into the currents flowing during neuronal activity. The dynamic clamp, which creates a programmable conductance, provides yet another probe – one that permits a sophisticated range of perturbations. Dynamic-clamp experiments allow simulations with biological neurons or the creation of hybrid circuits of biological and model neurons. The dynamic clamp breaks down barriers between mathematical modeling and experimental electrophysiology by allowing theorists to model 'in the dish' and experimentalists to perturb their system in ways that, perhaps, only a modeler would imagine. It is our hope that use of the method will continue to expand as new and clever applications are devised, and that these applications will continue to reveal new aspects and marvels of neural circuit dynamics.

Acknowledgements

Our research is supported by MH46742 and the Sloan/Swartz Center for Theoretical Neurobiology at Brandeis University.

References

1 Sharp, A.A. *et al.* (1993) The dynamic clamp: artificial conductances in biological neurons. *Trends Neurosci.* 16, 389–394
2 Sharp, A.A. *et al.* (1993) Dynamic clamp: computer-generated conductances in real neurons. *J. Neurophysiol.* 69, 992–995
3 Robinson, H.P. and Kawai, N. (1993) Injection of digitally synthesized synaptic conductance transients to measure the integrative properties of neurons. *J. Neurosci. Methods* 49, 157–165
4 LeMasson, G. *et al.* (1995) From conductances to neural network properties: analysis of simple circuits using the hybrid network method. *Prog. Biophys. Mol. Biol.* 64, 201–220
5 Hutcheon, B. *et al.* (1996) Models of subthreshold membrane resonance in neocortical neurons. *J. Neurophysiol.* 76, 698–714
6 Pinto, R.D. *et al.* (2001) Extended dynamic clamp: controlling up to four neurons using a single desktop computer and interface. *J. Neurosci. Methods* 108, 39–48
7 Manor, Y. and Nadim, F. (2001) Synaptic depression mediates bistability in neuronal networks with recurrent inhibitory connectivity. *J. Neurosci.* 21, 9460–9470
8 Butera, R.J. *et al.* (2001) A methodology for achieving high-speed rates for artificial conductance injection in electrically excitable biological cells. *IEEE Trans. Biomed. Eng.* 48, 1460–1470
9 Dorval, A.D. *et al.* (2001) Real-time linux dynamic clamp: a fast and flexible way to construct virtual ion channels in living cells. *Ann. Biomed. Eng.* 29, 897–907
10 Raikov, I. *et al.* MRCI: a flexible real-time dynamic clamp system for electrophysiology experiments. *J. Neurosci. Methods* (in press)
11 Lien, C.C. and Jonas, P. (2003) Kv3 potassium conductance is necessary and kinetically optimized for high-frequency action potential generation in hippocampal interneurons. *J. Neurosci.* 23, 2058–2068
12 Kullmann, P.H.M. *et al.* (2004) Implementation of a fast 16-bit dynamic clamp using LabView-RT. *J. Neurophysiol.* 91, 542–554
13 Le Masson, G. *et al.* (2002) Feedback inhibition controls spike transfer in hybrid thalamic circuits. *Nature* 417, 854–858
14 Chance, F.S. *et al.* (2002) Gain modulation from background synaptic input. *Neuron* 35, 773–782
15 Ulrich, D. and Huguenard, J.R. (1996) γ-Aminobutyric acid type B receptor-dependent burst-firing in thalamic neurons: a dynamic clamp study. *Proc. Natl. Acad. Sci. U. S. A.* 93, 13245–13249
16 Ulrich, D. and Huguenard, J.R. (1997) $GABA_A$-receptor-mediated rebound burst firing and burst shunting in thalamus. *J. Neurophysiol.* 78, 1748–1751
17 Cymbalyuk, G.S. *et al.* (2002) Bursting in leech heart interneurons: cell-autonomous and network-based mechanisms. *J. Neurosci.* 22, 10580–10592
18 Gramoll, S. *et al.* (1994) Switching in the activity of an interneuron that controls coordination of the hearts in the medicinal leech (*Hirudo medicinalis*). *J. Exp. Biol.* 186, 157–171
19 Kiehn, O. *et al.* (2000) Contributions of intrinsic motor neuron properties to the production of rhythmic motor output in the mammalian spinal cord. *Brain Res. Bull.* 53, 649–659
20 Hughes, S.W. *et al.* (1999) All thalamocortical neurones possess a T-type Ca^{2+} 'window' current that enables the expression of bistability-mediated activities. *J. Physiol.* 517, 805–815
21 Ma, M. and Koester, J. (1996) The role of potassium currents in frequency-dependent spike broadening in *Aplysia* R20 neurons: a dynamic clamp analysis. *J. Neurosci.* 16, 4089–4101
22 Harris-Warrick, R.M. *et al.* (1995) Dopamine modulation of two subthreshold currents produces phase shifts in activity of an identified motoneuron. *J. Neurophysiol.* 74, 1404–1420
23 Zhang, Y. *et al.* (2003) Overexpression of a hyperpolarization-activated cation current (Ih) channel gene modifies the firing activity of identified motor neurons in a small neural network. *J. Neurosci.* 23, 9059–9067
24 Swensen, A.M. and Marder, E. (2001) Modulators with convergent cellular actions elicit distinct circuit outputs. *J. Neurosci.* 21, 4050–4058
25 Turrigiano, G.G. *et al.* (1996) Cellular short-term memory from a slow potassium conductance. *J. Neurophysiol.* 75, 963–966
26 Goldman, M.S. *et al.* (2001) Global structure, robustness, and modulation of neuronal models. *J. Neurosci.* 21, 5229–5238
27 Bertram, R. *et al.* (2000) The phantom burster model for pancreatic β-cells. *Biophys. J.* 79, 2880–2892
28 Kinard, T.A. *et al.* (1999) Modulation of the bursting properties of single mouse pancreatic β-cells by artificial conductances. *Biophys. J.* 76, 1423–1435
29 Hughes, S.W. *et al.* (1998) Dynamic clamp study of I_h modulation of burst firing and delta oscillations in thalamocortical neurons *in vitro*. *Neuroscience* 87, 541–550
30 Sharp, A.A. *et al.* (1996) Mechanisms of oscillation in dynamic clamp constructed two-cell half-center circuits. *J. Neurophysiol.* 76, 867–883
31 Szucs, A. *et al.* (2003) Synaptic modulation of the interspike interval signatures of bursting pyloric neurons. *J. Neurophysiol.* 89, 1363–1377
32 Bartos, M. *et al.* (1999) Coordination of fast and slow rhythmic neuronal circuits. *J. Neurosci.* 19, 6650–6660
33 Elson, R.C. *et al.* (2002) Inhibitory synchronization of bursting in biological neurons: dependence on synaptic time constant. *J. Neurophysiol.* 88, 1166–1176
34 Joyner, R.W. *et al.* (1991) Unidirectional block between isolated rabbit ventricular cells coupled by a variable resistance. *Biophys. J.* 60, 1038–1045
35 Sharp, A.A. *et al.* (1992) Artificial electrical synapses in oscillatory networks. *J. Neurophysiol.* 67, 1691–1694
36 Velazquez, J.L.P. *et al.* (2001) Artificial electrotonic coupling affects neuronal firing patterns depending upon cellular characteristics. *Neuroscience* 103, 841–849
37 Elson, R.C. *et al.* (1998) Synchronous behavior of two coupled biological neurons. *Phys. Rev. Lett.* 81, 5692–5695
38 Prinz, A.A. *et al.* (2003) The functional consequences of changes in the strength and duration of synaptic inputs to oscillatory neurons. *J. Neurosci.* 23, 943–954
39 Manor, Y. and Nadim, F. (2001) Frequency regulation demonstrated by coupling a model and a biological neuron. *Neurocomputing* 38, 269–278
40 Derjean, D. *et al.* (2003) Dynamic balance of metabotropic inputs causes dorsal horn neurons to switch functional states. *Nat. Neurosci.* 6, 274–281
41 Wilders, R. *et al.* (1996) Model clamp and its application to synchronization of rabbit sinoatrial node cells. *Am. J. Physiol.* 271, H2168–H2182
42 Doiron, B. *et al.* (2001) Subtractive and divisive inhibition: effect of voltage-dependent inhibitory conductances and noise. *Neural Comput.* 13, 227–248
43 Mitchell, S.J. and Silver, R.A. (2003) Shunting inhibition modulates neuronal gain during synaptic excitation. *Neuron* 38, 433–445
44 Svirskis, G. *et al.* (2002) Enhancement of signal-to-noise ratio and phase locking for small inputs by a low-threshold outward current in auditory neurons. *J. Neurosci.* 22, 11019–11025
45 Blitz, D.M. and Regehr, W.G. (2003) Retinogeniculate synaptic properties controlling spike number and timing in relay neurons. *J. Neurophysiol.* 90, 2438–2450
46 Hanson, J.E. and Jaeger, D. (2002) Short-term plasticity shapes the response to simulated normal and parkinsonian input patterns in the globus pallidus. *J. Neurosci.* 22, 5164–5172
47 Carter, A.G. and Regehr, W.G. (2002) Quantal events shape cerebellar interneuron firing. *Nat. Neurosci.* 5, 1309–1318
48 Gauck, V. and Jaeger, D. (2000) The control of rate and timing of spikes in the deep cerebellar nuclei by inhibition. *J. Neurosci.* 20, 3006–3016
49 Jaeger, D. and Bower, J.M. (1999) Synaptic control of spiking in cerebellar Purkinje cells: dynamic current clamp based on model conductances. *J. Neurosci.* 19, 6090–6101
50 Harsch, A. and Robinson, H.P.C. (2000) Postsynaptic variability of firing in rat cortical neurons: the roles of input synchronization and synaptic NMDA receptor conductance. *J. Neurosci.* 20, 6181–6192
51 Destexhe, A. *et al.* (2001) Fluctuating synaptic conductances recreate *in vivo*-like activity in neocortical neurons. *Neuroscience* 107, 13–24
52 Reyes, A.D. *et al.* (1996) *In vitro* analysis of optimal stimuli for phase-locking and time-delayed modulation of firing in avian nucleus laminaris neurons. *J. Neurosci.* 16, 993–1007

Current Biology, Vol. 14, R661–R662, August 24, 2004, ©2004 Elsevier Ltd. All rights reserved. DOI 10.1016/j.cub.2004.08.012

Neural Networks: Models and Neurons Show Hybrid Vigor in Real Time

Dispatch

Astrid A. Prinz

Hybrid networks in which living neurons interact with digital or analog model neurons are providing insights into the role of neural and synaptic properties in shaping neural network activity.

Faced with the complexities of brain activity, some neuroscientists are turning to hybrid networks — neural networks consisting of living nerve cells interacting with model neurons — to help them understand how neural and synaptic properties shape the electrical activity of neural circuits [1,2] or to validate models of neurons in a network setting [3–5].

Neural activity is fundamentally complex. Neurons in networks with many synapses and feedback loops constantly receive inputs from other neurons, integrate them and generate electrical activity patterns in response. Network activity is thus shaped by interactions between the non-linear electrical properties of neurons and synapses. These complex interactions allow neural circuits to process information, support cognitive functions and control behavior.

Cellular electrophysiology experiments do not always acknowledge this complexity. Much of our understanding of neural circuits at the small network level relies on highly reductionist experiments. We characterize the response of isolated neurons to simple stimuli such as current injections or voltage steps, or we measure the signal transmitted through a single synapse. These time-proven experimental approaches are essential for our understanding of the building blocks of neural networks, but their reductionist nature raises the question whether we are missing something by probing a complex system with simple perturbations.

To examine the behavior of neurons and small networks under more realistic conditions, researchers in the early 90s began to study the interactions of living nerve cells with model neurons in hybrid networks [6,7]. Such connections between living and model neurons combine physiological realism with complete control over the neural and synaptic properties of the artificial network components. Hybrid networks thus create an interface between experimental and modeling studies, combining the best of both worlds [7].

The model neurons and synapses in hybrid networks can be digital or analog [7]. In hybrid networks with digital components, a technique called the ‘dynamic clamp’ [8,9] is used to monitor the membrane potential of living neurons, to numerically simulate model neurons and synapses on a computer, and to inject synaptic currents into living neurons in real-time, as if the living neurons were synaptically connected to the model neurons. Alternatively, the dynamic clamp can be used to insert artificial membrane conductances into living neurons embedded in a network, thus exploring the role of intrinsic conductances in shaping network output.

In hybrid networks with analog model neurons and synapses, a specially designed electronic circuit constitutes the artificial part of the network [10]. Such hardware model neurons and synapses are connected to living circuits through electrodes, creating a hybrid circuit that consists of a biological part and a dedicated silicon chip.

Electrical signalling in biological neurons occurs on many timescales, some as short as milliseconds. To be physiologically realistic, model neurons in hybrid circuits must interact with their living counterparts in real-time. For digital model neurons, this poses a challenge, especially if many digital components are to be included in a hybrid network. This is because the amount of real-time computation necessary for a hybrid network with digital model neurons scales with the number of model neurons and synapses involved, and quickly reaches the limit of current computer performance. In contrast, analog model neurons always operate in real-time, regardless how many model neurons participate in a hybrid circuit [7]. This scalability is a major advantage of hybrid networks with analog model components.

On the other hand, hybrid networks with digital model neurons are extremely flexible, because the artificial part of the network can easily be modified by re-programming the software that simulates the model neurons and synapses. In contrast, modifying the hardware circuit that emulates model neurons and synapses in a hybrid circuit with analog models often requires manufacturing a new chip [11], although a limited number of analog model parameters can usually be controlled by the experimenter [7].

Analog and digital model neurons also differ in their precision. While digital models operate essentially noise-free, analog model neurons are noisy and variable because of technical issues related to chip manufacture [11,12]. While variability and noise may be problematic, proponents of analog model neurons argue that they endow hybrid networks with a measure of realism [11] and can be exploited to test network activity for robustness [13].

In recent months, both types of hybrid network — with digital or analog model components — have become easier to implement because of newly developed real-time systems. The construction of hybrid networks with digital components is facilitated by the arrival of more user-friendly dynamic clamp systems [9]. And hybrid systems with analog model neurons can now be constructed using a simulation

Volen Center and Biology Department, Brandeis University, MS 013, 415 South Street, Waltham, Massachusetts 02454, USA. E-mail: prinz@brandeis.edu

platform based on biologically realistic electronic neurons [11]. These developments promise to increase the number of researchers that use the hybrid network method [7].

Most hybrid network applications fall into two categories. One group of studies investigates the role of neural and synaptic properties in shaping the behavior of a network, while another type of application uses hybrid networks to validate model neurons. Both approaches were combined in a recent study by Sorensen *et al.* [1], who coupled a bursting model neuron with a living interneuron in a half-center configuration to investigate the involvement of a membrane current, the hyperpolarization-activated inward current I_h, in pattern generation in the leech heartbeat timing network.

A half-center oscillator consists of a pair of mutually inhibiting neural oscillators that burst in alternation; such oscillators are involved in pattern generation for rhythmic behaviors such as breathing, swimming or chewing [14]. By varying the amount of I_h unilaterally in one part of their hybrid oscillator, Sorensen *et al.* [1] showed that I_h influences the frequency and activity pattern of the leech heartbeat half-center oscillator by regulating how long an oscillator stays in its inhibited phase. In addition, the authors demonstrated that the rhythmic pattern generated by the hybrid circuit was similar to the pattern generated by the biological circuit, thus validating their model of a leech heartbeat interneuron at a functional level not accessible to conventional experimental techniques.

In other recent examples of hybrid network applications, Nowotny *et al.* [2] used a hybrid circuit with an *Aplysia* neuron to show that spike-timing dependent plasticity enhances synchronization in neural networks, while Manor and Nadim [15] demonstrated that synaptic depression in neural networks with recurrent inhibition gives rise to bistability by combining a digital model neuron with a biological pacemaker neuron.

In a particularly elegant study, Le Masson *et al.* [16] reconstructed a thalamocortical circuit by coupling living neurons in the lateral geniculate nucleus to digital and analog model neurons. The researchers showed how feedback inhibition can functionally disconnect the cortex from sensory input in a state reminiscent of sleep, demonstrating the potential of the hybrid network approach in elucidating network function even in large circuits.

From a wider perspective, hybrid network investigations are part of a continuum of new experimental approaches towards brain investigation that range from the small network studies described here to brain–machine interfaces between external devices and neural circuits in behaving animals. Miguel Nicolelis [17] recently proposed to call these approaches ‘real-time neurophysiology’, emphasizing the need to operate at the time-scale of neural activity when interacting with neural tissue. Hybrid systems at all levels of neural organization have the potential to complement more traditional neurophysiological methods and to further our understanding of complex neural processes.

References

1. Sorensen, M., DeWeerth, S., Cymbalyuk, G., and Calabrese, R.L. (2004). Using a hybrid neural system to reveal regulation of neuronal network activity by an intrinsic current. J. Neurosci. *24*, 5427-5438.
2. Nowotny, T., Zhigulin, V.P., Selverston, A.I., Abarbanel, H.D.I., and Rabinovich, M.I. (2003). Enhancement of synchronization in a hybrid neural circuit by spike-timing dependent plasticity. J. Neurosci. *23*, 9776-9785.
3. Aliaga, J., Busca, N., Minces, V., Mindlin, G.B., Pando, B., Salles, A., and Sczcupak, L. (2003). Electronic neuron within a ganglion of a leech (Hirudo medicinalis). Phys. Rev. E 67, Art. No. 061915.
4. Pinto, R.D., Varona, P., Volkovskii, A.R., Szucs, A., Abarbanel, H.D.I., and Rabinovich, M.I. (2000). Synchronous behavior of two coupled electronic neurons. Phys. Rev. E *62*, 2644-2656.
5. Szucs, A., Varona, P., Volkovskii, A.R., Abarbanel, H.D.I., Rabinovich, M.I., and Selverston, A.I. (2000). Interacting biological and electronic neurons generate realistic oscillatory rhythms. Neuroreport *11*, 563-569.
6. Yarom, Y. (1991). Rhythmogenesis in a hybrid system — interconnecting an olivary neuron to an analog network of coupled oscillators. Neuroscience *44*, 263-275.
7. LeMasson, G., LeMasson, S., and Moulins, M. (1995). From conductances to neural network properties: Analysis of simple circuits using the hybrid network method. Prog. Biophys. Mol. Biol. *64*, 201-220.
8. Sharp, A.A., O'Neil, M.B., Abbott, L.F., and Marder, E. (1993). Dynamic clamp: computer-generated conductances in real neurons. J. Neurophysiol. *69*, 992-995.
9. Prinz, A.A., Abbott, L.F., and Marder, E. (2004). The dynamic clamp comes of age. Trends Neurosci. *27*, 218-224.
10. Mahowald, M., and Douglas, R. (1991). A Silicon Neuron. Nature *354*, 515-518.
11. Renaud-Le Masson, S., Le Masson, G., Alvado, L., Saighi, S., and Tomas, J. (2004). A neural simulation system based on biologically realistic electronic neurons. Inf. Sci. *161*, 57-69.
12. Rasche, C., Douglas, R., and Mahowald, M. (1998). Characterization of a pyramidal silicon neuron, neuromorphic systems: engineering silicon. In Neurobiology. L.S. Smith, and A. Hamilton, eds. (Teaneck, NJ: World Scientific), pp. 169-177.
13. Cymbalyuk, G.S., Patel, G.N., Calabrese, R.L., DeWeerth, S.P., and Cohen, A.H. (2000). Modeling alternation to synchrony with inhibitory coupling: A neuromorphic VLSI approach. Neural Comput. *12*, 2259-2278.
14. Hill, A.A., Van Hooser, S.D., and Calabrese, R.L. (2003). Half-center oscillators underlying rhythmic movements. In The handbook of brain theory and neural networks. M. Arbib, ed. (Cambridge, MA: MIT), pp. 507-510.
15. Manor, Y., and Nadim, F. (2001). Synaptic depression mediates bistability in neuronal networks with recurrent inhibitory connectivity. J. Neurosci. *21*, 9460-9470.
16. Le Masson, G., Renaud-Le Masson, S., Debay, D., and Bal, T. (2002). Feedback inhibition controls spike transfer in hybrid thalamic circuits. Nature *417*, 854-858.
17. Nicolelis, M.A.L. (2003). Brain-machine interfaces to restore motor function and probe neural circuits. Nat. Rev. Neurosci. *4*, 417-422.